Technical University of Crete
School of Electronic and Computer Engineering

Analysis and Quantification of Spatiotemporal Features of Diagnostics Importance in Cervical Neoplasia

Androula Savva

Committee

Professor Balas Costas (Supervisor)
Professor Zervakis Michalis
Associate Professor Lagoudakis Michail

Chania 2015

Abstract

Cervical cancer is the fourth most common malignant disease in women worldwide. It poses a major threat, especially in developing regions, due to the high cost of screening and treatment, as well as the lack of fast, accurate diagnostic methods. Acetowhitening (AW) is a phenomenon observed after the application of an acetic acid (AA) solution on the cervix. Acetic acid interacts with pre-cancerous cells of the epithelium, altering the tissue's scattering characteristics and causing abnormal cells to appear opaque. As part of the diagnostic chain, both Pap test and colposcopy, suffer from low sensitivity, since visual assessment of AW is subjective, qualitative and depends heavily on the visual acuity and training of the examiner. Quantitative, objective assessment of AW characteristics was first presented in DySIS™, a novel instrumentation developed in the late 90's. DySIS™ acquires a sequence of images over time, recording the development of the AW phenomenon. In this thesis, we present a novel algorithm that extracts features of diagnostics importance by exploiting only spatial information and is based on a physics model that encapsulates the basic biochemical procedures producing the AW. Using a single snapshot of the cervix, 144 seconds after the application of the AA solution and without prior knowledge, we identify the area and grade of the lesions utilizing bio optical properties of the tissue. The introduced method is fast, cheap and achieves high sensitivity (80%) and specificity (79%), simplifying the current diagnostic chain and showing promising results in aiding screening especially for low resource see and treat facilities.

Table of Contents

1   Introduction

1.1   Cervical cancer: Epidemiology and risk factors

Cervical cancer is the fourth most common malignant disease in women worldwide. Estimates indicate that in 2012, 528.000 new cases occurred while 266.000 women died of cervical cancer. Cervical cancer poses a major threat in less developed countries. Approximately 85% of all new cases and 87% deaths by cervical cancer, occur in regions such as Eastern Africa, Melanesia, southern Africa etc [1].The high cost of diagnosis and treatment of pre-cancerous conditions along with the lack of fast, simple and accurate methods of screening seems to be the main factor for the high rates of incident and mortality in such areas.
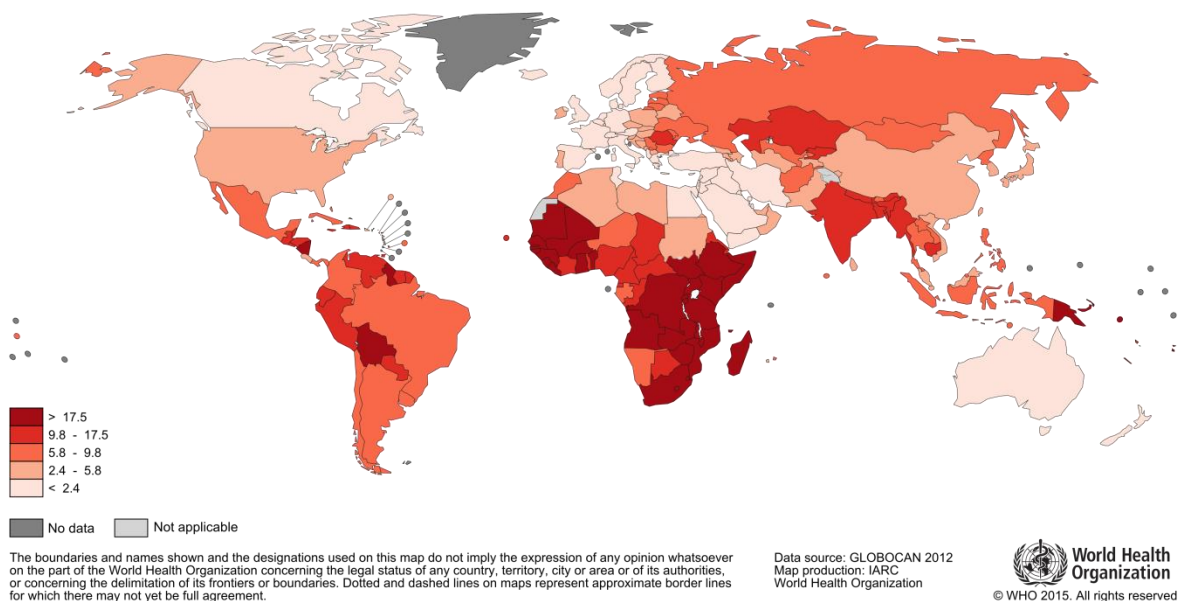
Figure 1.1-1 Estimated Cervical Cancer Mortality Worldwide in 2012 [1]

There are several histologic subtypes of cervical cancer:

- squamous cell carcinoma (about 80-85% of cases)
- adenosquamous carcinoma
- small cell carcinoma
- neuroendocrine tumour
- glassy cell carcinoma
- villoglandular adenocarcinoma

Though squamous cell carcinoma is the one with the highest incidence.

Chronic infection of Human Papillomavirus (HPV) has been found to be the leading cause of precancerous cervical lesions. Certain HPV types (high risk strains) appear to be involved in the development of more than 90% of cases. The most common high risk strains of HPV are types 16 and 18, which are known to cause about 70% of all cervical cancers.

Genital HPV types are transmitted through sexual contact, although penetration is not necessary. The use of condom does not suffice for protection, since skin to skin contact of the genital area can also lead to infection [3].Most sexually active women will, at some point of their life, be infected from HPV. In most cases, the immune system eliminates HPV and clears the infection. But in some women, the infection persists and leads to cervical dysplasia.

Cervical dysplasia is a pre-cancerous condition in which abnormal cell growth occurs on the epithelial cells of the cervix or endocervical canal. While these abnormal cells (called cervical intra-epithelial neoplasia or CIN) are not cancerous per se, they may lead to cancer.

Based on the extent of cell abnormality, CIN is divided into three grades [4]:
- CIN1 indicates mild changes, affecting one third of the thickness of the epithelium layer of the cervix
- CIN2 indicates moderate dysplasia, affecting two-thirds of the thickness of the epithelium
- CIN3 indicates severe dysplasia to carcinoma in situ that spans more than 2/3 of the epithelium.

The aforementioned classification is used to indicate the volume of abnormal cells affecting the cervix.
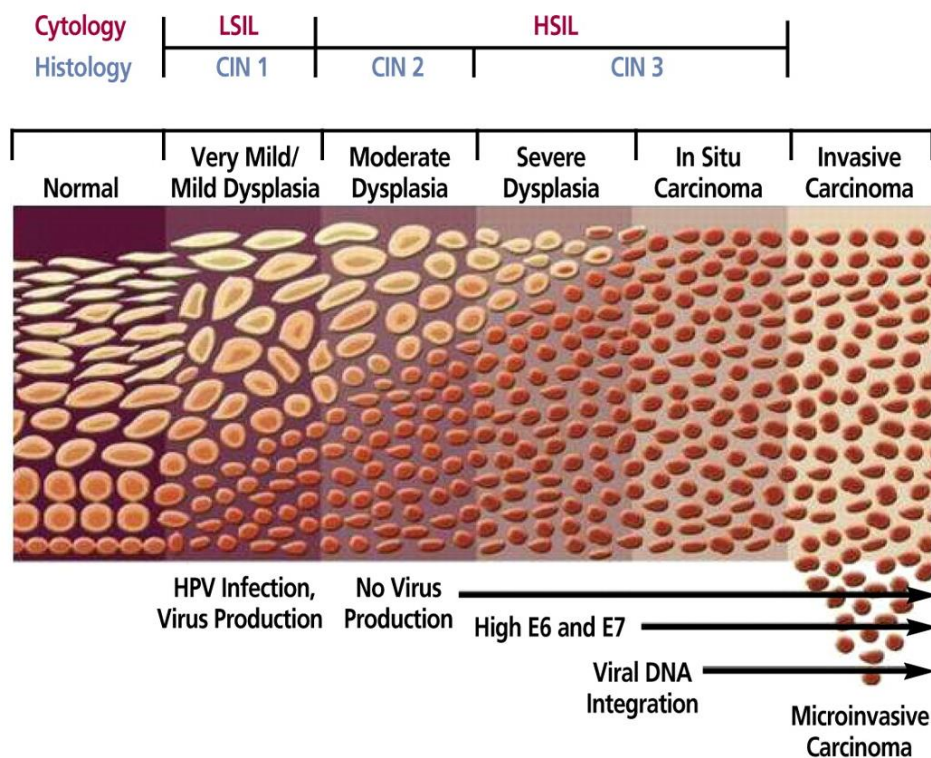
Figure 1.1-2 Progression from a benign cervical lesion to invasive cervical cancer

Cytology characterizes CIN1 or less severe lesions as Low Grade Squamous Lesions (LSIL), which usually regresses back to normal without treatment. Both CIN2 and CIN3 are high grade lesions and are characterized as High Grade Squamous Intraepithelial Lesion (HSIL).The discrimination between HSIL and LSIL lesions is crucial for the lesion's management decision-making (follow-up or immediate treatment respectively).

1.2 Diagnosis and Treatment

1.2.1 Diagnostic Chain

Routine screening is an essential part in a woman's health care and has been proven to minimize the incidence and mortality of cervical cancer, due to the early detection of abnormal cells. Latest screening recommendations from the American Cancer Society indicate that all women should begin cervical cancer screening at the age of 21. Pap test must be repeated every 3 years unless more frequent tests are recommended by a doctor. Women who are at high risk for cervical cancer may need to be screened more often [5].

Over the years, a standard method has been established for preventing cervical cancer; cytology screening, colposcopic examination and subsequent biopsy sampling of abnormal screening results, and finally, treatment of the pre-cancerous abnormalities.

Cytology screening

Cytology screening, known as Pap test, is the very first step in the diagnostic chain. Pap test is a procedure used to collect cells from the cervix, which are then carefully examined in order to detect abnormal changes. It is a simple, painless and low cost procedure [6, 7].

During the test, the patient lies on her back on the examination table. The doctor gently inserts a speculum into the patient's vagina in order to widen it. Cells from the surface of the cervix are collected using a soft, narrow brush or spatula. A small brush or a cotton-tipped swab is then inserted into the opening of the cervix to take a sample from the inner part.

The cell samples are placed onto a glass slide, sprayed with a preservative and then analyzed under a microscope by a cytopathologist.
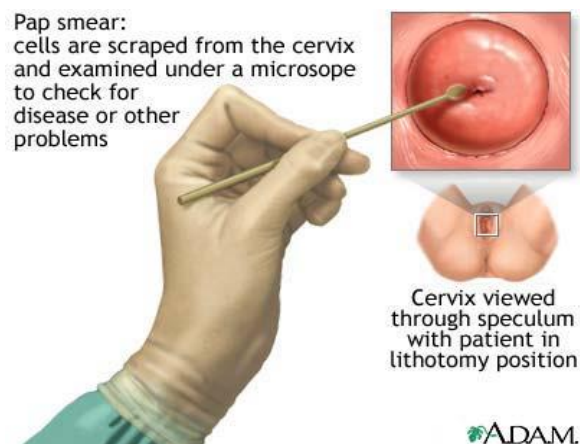
Figure 1.2-1 Pap test procedure

Abnormal squamous cell Pap test results are reported using the Bethesda system, introduced in 1988 and revised in 1991 and 2001 [11].

Table 1.2.1-1: Bethesda system

Bethesda system result	Description
atypical squamous cells (ASC)	Cells don't look normal.
atypical squamous cells – undetermined significance (ASC-US)	Some cells don't look completely normal. It's not clear what the cell changes mean.
low-grade squamous intraepithelial lesion (LSIL)	Cells don't look normal, but they usually aren't precancerous. Considered a mild abnormality.
atypical squamous cells – cannot rule out high-grade squamous intraepithelial lesion (ASC-H)	Cells don't look normal. It's not clear what the cell changes mean, and a high-grade lesion can't be ruled out. The abnormal change may be precancerous.
high-grade squamous intraepithelial lesion (HSIL)	There are abnormal, or precancerous, cells present. The cells may develop into cancer if they aren't treated.
squamous cell carcinoma (SCC)	There are cancerous cells present.

If a Pap test indicates presence of abnormal cells, the patient is referred for colposcopy, otherwise, regular pap tests should be continued according to the guidelines.

Colposcopy

Colposcopy was introduced in 1960 as a confirmatory test, for evaluation of women with abnormal cervical cytologic findings. It is a procedure for the examination of the cervix, used to verify the presence of an abnormality, define the severity and to help determine what the appropriate treatment is [8, 9].

A colposcope, a specialized piece of equipment, provides strong lighting and magnification allowing the cervix to be closely examined. The colposcope doesn't enter the vagina and remains outside the patient's body. Latest colposcopes have a camera attached, projecting images on a small screen.

Colposcopic examination is based on the visual examination of the tissue with the aid of a low magnification microscope. Similarly to a routine pelvic examination, the patient lies on her back and the doctor widens the vagina using a speculum. In order to highlight abnormal areas, topical application of acetic acid solution 3-5% is routinely used as a contrast agent, for more than 70 years. The solution washes away mucus covering the epithelial surface and interacts with the tissue, generating an optical signal perceived as transient tissue whitening. Clinical evidence supports that the degree and duration of the latter is associated with the lesion's grade and the

phenomenon is known as acetowhitening (AW) effect. Colposcopists evaluate the intensity and density of the acetowhitening reaction to assess the severity of the lesion.
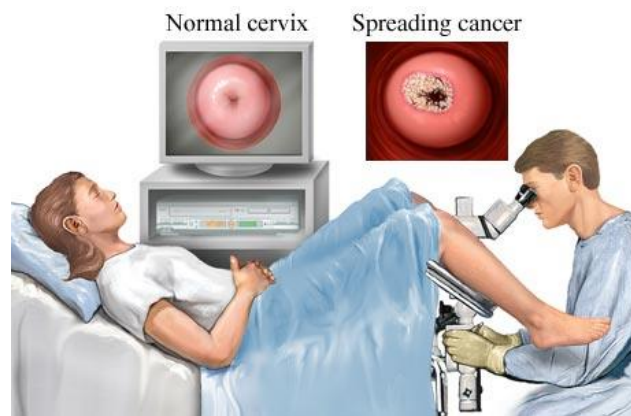
Figure 1.2-2 Colposcopy examination

Biopsy

If, during the colposcopy, any abnormal areas are detected, a small sample of tissue (biopsy) may be removed for closer examination. Samples may be taken from areas that appeared as white due to the application of the acetic acid, other areas that look suspicious and even random points [10].

Usually, the doctor performs a punch biopsy, where a scissors-like instrument (biopsy forceps) is inserted through the speculum or colposcope and is used to snip tiny specimens approximately the size of half a grain of rice, from selected sites on the cervix. The samples are examined under a microscope for changes in the cells. If a sample of tissue is needed from inside the opening of the cervix (the endocervical canal), a test called endocervical curettage (ECC) will be performed. Since the endocervical canal cannot be seen by the colposcope, a small sharp-edged tool called a curette is gently put into the endocervical canal to take a sample [12].
Results of biopsy are classified as normal, cervical intraepithelial neoplasia or invasive carcinoma. Cervical intraepithelial neoplasia is furthermore classified as CIN1, CIN2 or CIN3, as previously described.

Rare complications associated with cervical punch biopsy include excessive bleeding for up to a week after the procedure and infection. Mild cramping, vaginal soreness, and dark discharge for 1–3 days may occur.

1.2.2 Treatment of abnormal cervical cells

The aim of treatment is to remove or destroy the abnormal cervical cells while preserving as much normal tissue as possible. There are several methods used nowadays, each one depending on the type of abnormal cells and the severity of the cervical lesion.
CIN1 abnormalities do not need to be treated, since there is a strong possibility that the cells will regress to normal, although regular screening is necessary.

Treatment for higher grade CIN involves removal or destruction of the neoplastic cervical cells by cryotherapy, laser therapy, loop electrical excision procedure (LEEP/LLETZ), cone biopsy or hysterectomy.

LEEP is the most common treatment of pre-cancerous lesions. It is essentially the removal of the transformation zone, where cellular abnormalities typically occur. This method involves using a wire loop, through which an electric current is passed, to remove the abnormal cells.
The cervical transformation zone and lesion are excised to an adequate depth. During LEEP, only a small amount of normal tissue is removed at the edge of the abnormal tissue area.
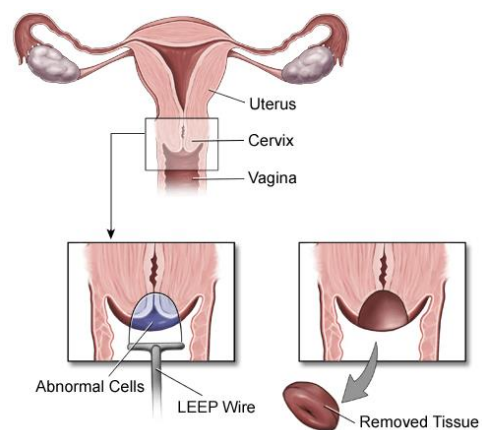
Figure 1.2-3 Loop electrical excision procedure

Much like LEEP, a cone biopsy involves removing a part of the cervix, although somewhat larger and cone-shaped. The widest part of the cone is taken from the opening of the cervix, while the middle and tip of the cone are taken from the cervical canal leading to the uterus. Though these procedures are typically used for treatment, they can also be used as part of the diagnosis since the abnormal tissue is excised and not destroyed.
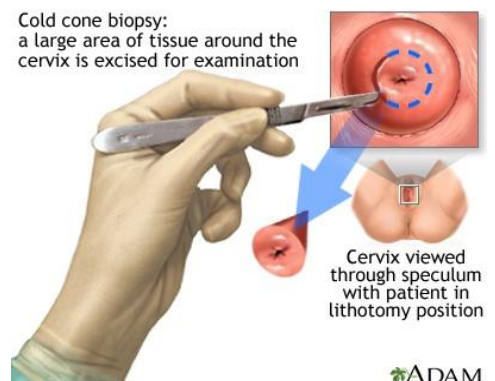
Figure 1.2-4 Cold cone biopsy procedure

In cryotherapy, a steel instrument is cooled to subzero temperatures by immersion in liquid nitrogen and then applied to the surface of the cervix. The cells are frozen and eventually die.
In laser therapy, a laser beam is used to destroy abnormal cells at the surface of the cervix.
Since cryotherapy and laser therapy destroy the abnormal cells, further examination is not possible.

1.2.3 Reliability and accuracy of the diagnostic chain

Although the latter methods have been proven to be effective for the prevention of cervical cancer, they are not perfect. One of the greatest limitations of both Pap test and colposcopy is the human factor. Results need to be examined by humans, therefore an objective analysis is not always possible.

Cervical smear is the primary screening method for cervical neoplasia and has reduced the mortality of cervical cancer remarkably. However, it is not a perfectly reliable measure considering that it has low sensitivity (~59%), led by both sampling and reading errors.
Traditional colposcopy also exhibits significant limitations when it comes to diagnosing pre-cancerous lesions. Visual assessment of macroscopic features of diagnostic importance, including the AW pattern, is subjective, qualitative and depends heavily on the visual acuity and training of the examiner. Therefore, colposcopy suffers from low sensitivity (55-65%) and specificity (70-90%), and is responsible for 52% of screening failures, including missed lesions, unnecessarily repeated tests and diagnostic delays.

At the same time, both of these methods seem to be responsible for the cause of anxiety in a lot of patients, regarding both the time needed for results to be available and the frequency of the tests. This explains why so many women avoid to be regularly screened.

There is high need in developing novel methods and instrumentation, in order to achieve high accuracy and objectiveness. It is also imperative to minimize the psychological impact on patients with simple and fast diagnostic methods.

1.3 Thesis Contribution

In this thesis, an innovative algorithm is proposed for identifying pre-cancerous lesions based on Dynamic Spectral Imaging. We attempt to transfer feature extraction from time to space, utilizing only a single frame for the detection of abnormal areas. Due to the complexity of the problem and the dimensionality reduction from time to space, feature extraction was performed on a single frame and was based only on the ascetowhitening phenomenon.
The algorithm is based on a physics model that encapsulates the basic biochemical procedures producing the AW. Using a single snapshot of the cervix, 144 seconds after the application of the AA solution and without prior knowledge, we successfully identify the area and grade of the lesions utilizing bio optical properties of the tissue.
We have successfully minimized the time as well as the data needed for the identification and categorization of the lesions, thus providing, for the first time, a complete method able to be used in low resource see and treat facilities for the early and low-cost screening for cervical cancer.

1.4   Chapters Summary

In the following chapters, we explain the bio physical, bio optical background behind the conception of the method as well as the entire process followed, step by step, for the implementation of the algorithm.

In Chapter 2, we explore the method upon which our proposal is based on, a novel instrumentation developed in the late 90s which exploits Dynamic Spectral Imaging. A detailed description of both the technology and methodology of the DySIS™ instrumentation is discussed.

The biological background associated with the present thesis is examined in Chapter3, where the anatomical and structural characteristics of the cervix are explained. A detailed explanation of the development of Cervical Intraepithelial Neoplasia is given, emphasizing in the alteration of the aforementioned characteristics.

The method proposed in the present thesis is strictly associated with a biophysical model, which is unraveled in Chapter 4. Procedures such as light-tissue interaction as well as the physical properties of the light are further on analyzed.

In Chapter 5, we explain in detail the methodology, reporting the intermediate results of the algorithm, starting with the main body of the algorithm, and we propose several methods that were used for optimization.

In Chapter 6, a statistical analysis is performed, in order to evaluate the effectiveness of the proposed algorithm in detecting pre-cancerous lesions. Not only we compare DySIS™, colposcopy and the proposed algorithm, we also examine differences between several different versions of the algorithm.

Finally, in Chapter 7, we conclude our approach and outline the importance of the proposed algorithm. A brief reference of the possible future work we expect to be made is also outlined.

2 DySIS™: A novel approach

In order to compensate for the deficiencies of the present screening methodology, C. Balas et al developed in the late nineties a novel dynamic, contrast-enhanced optical imaging instrumentation, able to quantitatively measure and map the effects of the acetic acid [17, 18].

By exploiting the unique interaction of acetic acid on abnormal cells, the Dynamic Spectral Imaging System - DySIS™- emerged as an assistive method for the conventional colposcopy, aiming to enhance the diagnostic stage of the cervical cancer prevention program, reduce missed lesions and diagnostic delays.

Dynamic Spectral Imaging was developed for measuring and modeling the uptake kinetics of biomarkers in vivo, through the dynamic optical signals generated.

Acetic acid has been used for over 70 years empirically for assisting the visualization of abnormal sites of the uterine cervix, but was first investigated in late 1990's as a biomarker.

DySIS™ utilizes the interaction of acetic acid with neoplastic cells, by measuring the alterations in tissue optical characteristics as a function of time and at specific spectral bands and for every image pixel. In the case of cervical epithelium the obtained dynamic optical data are correlated with the neoplasia grade, thus enabling the unbiased differentiation between, neoplastic and not, lesions, as well as between neoplasias of different grades. It allows the spatiotemporal recording of the induced biological events and processes, in vivo, non-invasively and in real time.

The efficacy of this novel instrumentation was proven in two international clinical trials, demonstrating an improvement in diagnostic sensitivity (~63%) over Papanicolaou test and colposcopy.

Figure 1.4-1 DySIS™ Colposcope

2.1 Acetowhitening Phenomenon

Acetowhitening phenomenon is manifesting in abnormal cells after the infusion of acetic acid solution in the tissue. Studies have shown that the dynamic characteristics of the optical signal recorded during the phenomenon are directly related with both the percentage of neoplastic cells of the tissue as well as their abnormal metabolic activities [19]. This correlation of the backscattered light and the population of infected cells grants the capability of identifying the neoplasia stage (CIN I, II, III).

Glycolysis, taking place in the cytosol of cells, is a metabolic pathway where a glucose molecule is dissolved into pyruvic acid (2.1) and is the fundamental energy source of a cell.

$$C_6H_{12}O_6 \rightarrow CH_3COCOO^- + H^+ \qquad (2.1)$$

Neoplastic cells reproduce with faster than normal rate, thus demand more volumes of oxygen. This lack of oxygen forces pyruvic acid to dissolve into lactic acid (2.2), which is emitted in the extracellular space.

$$CH_3COCOOH \rightarrow 2C_3H_6O_3 \qquad (2.2)$$

In order for a given, neoplastic or not, cell to maintain its functionality, pH value must lie between 7 and 7.5, which is considered normal pH. This leads to acidic extracellular space around neoplastic cells, allowing slow accumulation of weak acids in the intracellular space, which are constantly ionized. The cellular membrane is impregnable to charged particles thus entrapping the ions within the cells ("ion trapping").

When infusing acetic acid in the tissue, it is instantly ionized producing salt and a hydrogenation (2.3).

$$CH_3COOH \leftrightarrow CH_3COO^- + H^+ \qquad (2.3)$$

Ionization of the acetic acid is a duplex chemical reaction, thus governed by Le Châtelier's principle (Equilibrium Law):

"If a chemical system at equilibrium experiences a change in concentration, temperature, volume or partial pressure the equilibrium shifts to counteract the imposed change and anew equilibrium is established."

Obeying this principle, acetic acid is passively diffused unionized inside neoplastic cells, where pH regulation mechanisms of the cell kick in. As a result, there is high concentration of hydrogen cations, which transubstantiate the proteins inside the cellular core, reversibly altering the scattering characteristics of the core. This is a reversible procedure and within few moments the tissue regains its original characteristics once intracellular pH levels return to normal.
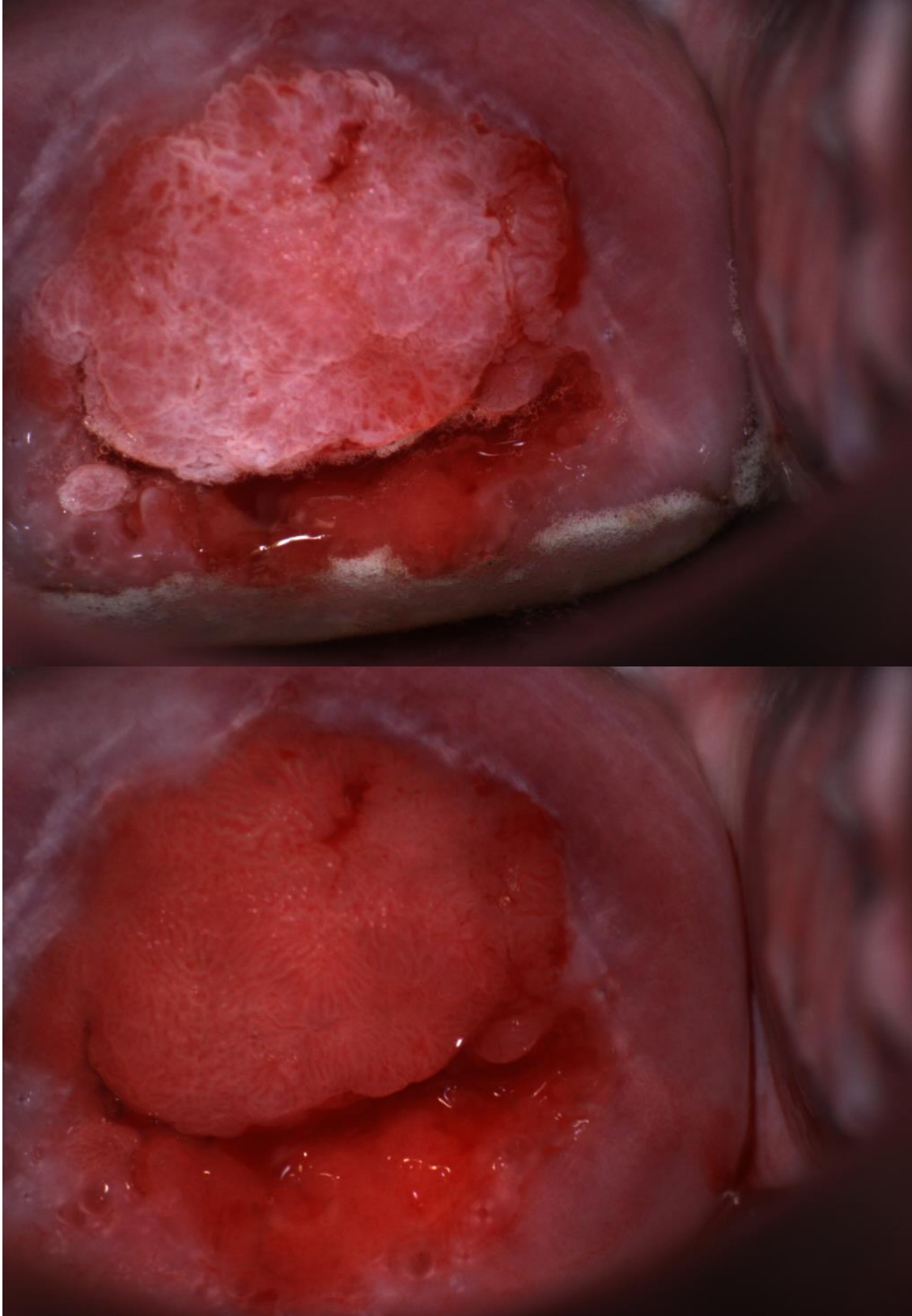
Figure 2.1-1 Effects of acetic acid application (acetowhitening phenomenon) a) before the application (upper image) b) 144seconds after the application (below image)

2.2 Technology and Instrumentation

The DySIS™ integrates an optical imaging head supported by a mechanical basis, which includes weight counter balancing and space translating mechanisms. The basis allows for the easy manual positioning of the optical imaging head to obtain a sharp image of the tissue and includes mechanical and electromagnetic brakes that are manually activated through a trigger, once the optimum field-of-view has been achieved. In order to maintain approximately the same field-of-view throughout the entire examination procedure, the optical imaging head is detachably connected through a mechanical shaft attached to a vaginal speculum. Once the latter has been inserted into the vagina, its blades are opened to enable the visualization and the imaging of the cervix of the uterus.

Tissue imaging is performed with the aid of a 35 mm lens, coupled with a 1024X768, 8bit/channel color CCD camera. The camera is interfaced with a dual core microprocessor computer unit, through a fire-wire (IEEE-1394) cable. The optical imaging head further comprises a white Light Emission Diode (LED), coupled with light collimating and focusing optics for uniform tissue illumination. A pair of polarizers, one disposed at the imaging and one at the illumination pathways having their polarization axes perpendicular with each other, is employed for the cutting-off of the surface reflection originating from the air-tissue interface and of the glare originating from the mucus. The optical head has been configured to capture images from a 23mm X 20mm tissue area, including the entire transformation zone of the cervix. Assuming an average 35μm cell diameter and given the aforementioned sensor's spatial resolution, it can be easily calculated that the backscattered light intensity recorded by a given pixel, corresponds approximately to the area occupied by a single cell.

Technical evaluation shows that the sensor has a substantially linear response across its entire dynamic range. In order to ensure device independent and reproducible imaging, systems calibration is performed a using Ba_2SO_4 calibration plate, with unity reflectance across the visible spectral range.

2.3 Data collection

The initiation of the image capturing process is triggered by the acetic acid applicator, in order to ensure synchronization between them. A reference image is captured prior to the application of the acetic acid solution, which is followed by an automatic image capturing during the evolution of the AW phenomenon. Images are captured with a frequency of 7 seconds and for a total time of 240 second.

The captured images are then aligned using an embedded registration algorithm, in order to compensate for both image translations and deformations, caused by tissue's contractions and patient's movement respectively. From the captured images stack, and particularly, from their green channel, the diffuse reflectance (DR) curves are calculated for every image pixel, expressing the temporal characteristics of the AW phenomenon. Based on the DR curves, a series of features are then calculated, such as time integral, DR peak value (DR_{max}) etc. A pseudocolor map is then

generated, with different colors representing different feature values, which is overlaid onto the real-time displayed color image of the cervix. This allows for the direct comparison of the feature values, corresponding to the biopsied tissue area with the histological results, thus, enabling their direct comparison with histological classification. Based on this procedure, the evaluation of the diagnostic value of the derived dynamic optical parameters is enabled.
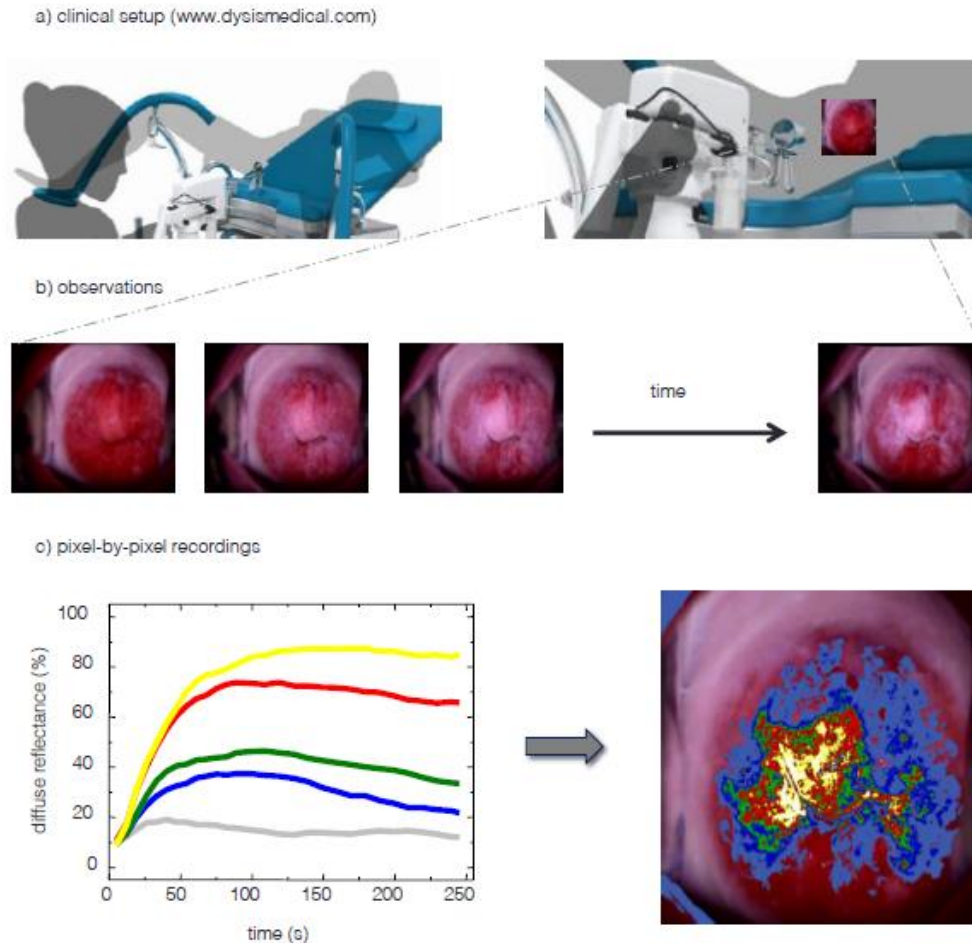
Figure 2.3-1 (a) After calibration the patient is placed in the lithotomy position and the vaginal speculum is inserted, thus enabling the visualization of the cervix. (b) Image capturing sequence. (c) Diffuse-reflectance curves for every image pixel, expressing the temporal characteristics of the AW phenomenon. From the corresponding integrals a pseudocolor map is generated and overlaid onto the real-time displayed color image of the cervix.

The greatest advantage of DySIS™ is that it eliminates the subjectivity inherent in current diagnostic procedures (cytology and colposcopy), since it is an automated procedure. Therefore, incorrect diagnoses of lesions are minimized, eliminating the extreme burden on both patients and health care systems. DySIS™ performs a rapid, quantitative and side effect-free examination procedure to provide in-vivo topography of the lesion. As such, DySIS™ technology emerges as an indispensable tool for the diagnosis, screening and follow up, and for the on-line guiding of biopsy sampling and surgical treatment.

2.4 Clinical Studies

Two independent, large, multicenter studies took place in order to test DySIS™, resulting into three peer-reviewed publications.

1st Clinical Trial

The first clinical trial [20] took place in the colposcopy clinics of Hammersmith Hospital and St Mary's Hospital, London, United Kingdom and at the Alexandra Hospital, Athens, Greece. Initially, 529 women were recruited during the period May 2004 and July 2005; of those, 82 were recruited to the training group from May to July 2004. The remaining 447 women were recruited to the test group between August 2004 and July 2005; of those, 139 women were excluded, leaving only 308 women eligible.

All eligible members of the validation group (308 women) had an abnormal pap-test and had been referred for colposcopy. The diagnostic performance of DySIS™ was compared against cytology (Pap test) and colposcopy, using histology as the "golden standard". There was no interference between the DySIS™ scan and the operator's assessment, since the grading of the lesion was performed in an automated basis, according to the protocol.

Traditional colposcopy missed 37 out of the 72 patients with high-grade disease, achieving a sensitivity of merely 49%. The DySIS™ scan identified an additional 22 patients with high-grade (CIN2+) disease delivering a sensitivity of 79%, indicating the better performance of DySIS™ over traditional colposcopy.

2st Clinical Trial

The aim of the second clinical trial [21] was to examine whether the performance of DySIS™ would be further improved by combining both DySIS™ and conventional colposcopic examination. The trial took place in three Dutch Hospitals; the VU University Medical Centre in Amsterdam, the Reinier de Graaf Hospital in Voorburg and the St. Antonius Hospital in Nieuwegein.

In total 275 women were included in the study: 183 women were analyzed in the 'according-to-protocol' (ATP) cohort and 239 women in the 'intention-to-treat' (ITT) cohort. The published results confirmed the findings of the 1st trail.

In the ATP cohort, the sensitivity of DSI colposcopy to identify women with high-grade (CIN2+) lesions was 79% and the sensitivity of conventional colposcopy was 55%. Moreover, it was found that when DySIS™ is used as an adjunct to conventional colposcopy, the combined sensitivity reaches the value of 88% but at a more (as compared with the first study) significant cost in specificity (69%).

3   Biological Background

3.1   Anatomy of the cervix

The cervix is the lower, narrow part of the uterus in the human female reproductive system. It is cylinder shaped with radius approximately 2.5 cm and is covered by smooth, moist tissue, which consist the epithelium of the cervix. It acts as a physical barrier between the external environment (vaginal canal) and the uterus [22-27].

The opening into the uterus is called internal os and the opening into the vagina is called external os. Within the cervix itself, the anatomy is subdivided into the endocervix and the ectocervix. The endocervix (endocervical canal) is a luminal cavity within the cervix, forming a passageway between the external os and the internal os. It is lined by a mucus-secreting simple columnar epithelium. The ectocervix is the portion of the cervix that projects into the vagina. It is lined by stratified squamous non-keratinized epithelium, extending onto the lip of the cervix. The opening in the ectocervix, the external os, marks the transition from the ectocervix to the endocervical canal.
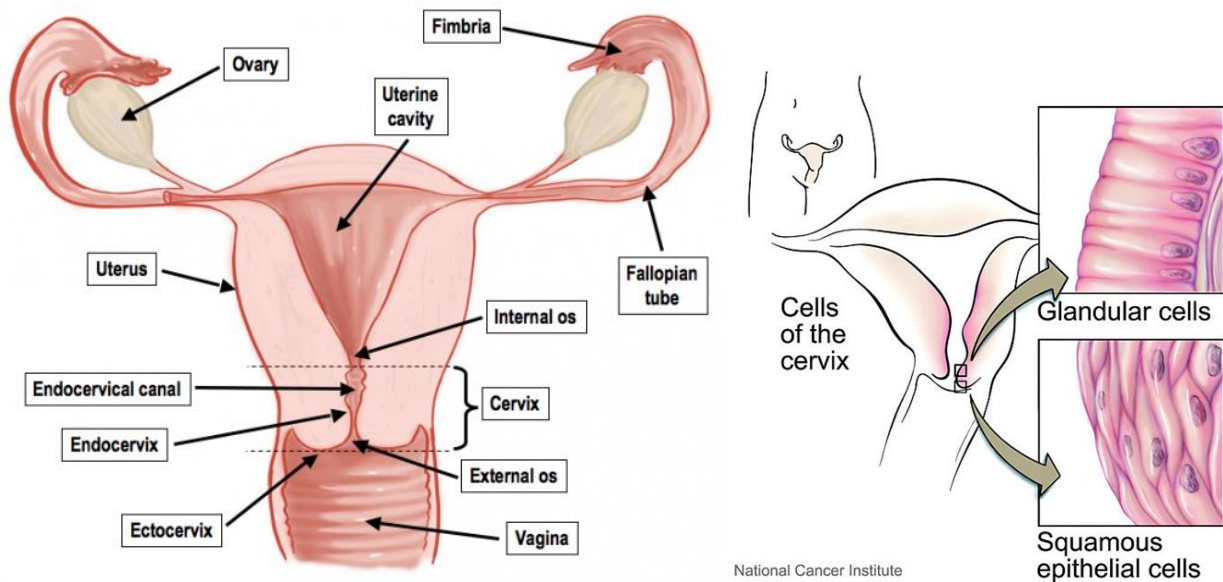
Figure 3.1-1 Anatomy of the female human reproductive system

3.2 Function

The cervix carries out many critical functions that contribute to the overall reproductive health and wellbeing of women. It allows the passage of menstrual fluid, promotes fertility and protects the uterus and upper reproductive tract from pathogens.

Throughout the menstrual cycle, the cervix changes in size, location and texture. Hormonal changes, such as rising of estrogen prior to ovulation, cause the cervix to swell and soften and the external os to dilate. During this time, mucus secreting from the endocervical canal, turns thin and serous, acting as a transport medium to spermatozoa, and is more alkaline and hence more hospitable to sperm.

After ovulation, progesterone causes the cervix to harden and close. The mucus turns thick and more acidic, creating a hostile environment for the sperm, preventing it from entering the uterus. Thick mucus also acts as a plug and prevents any bacteria or pathogens from entering the uterus.

The cervix also plays a major role in childbirth. During the preparation of birth, as the fetus descends, the head rests on and is supported by the cervix. The cervix becomes softer and shorter, begins to dilate and rotates to face anteriorly. During childbirth, the cervix dilates to a diameter of more than 10cm to accommodate the head of the fetus, as it descend from the uterus to the vagina.

3.3 Structure

Generally, the cervix is covered by two epithelial tissue types; the columnar epithelium and the stratified squamous epithelium.

Squamous epithelium is non-keratinizing and is composed of a continuous layer of stratified (multi-layered) flat, polygonal cells with centrally located nuclei. The stratified squamous epithelium is divided into four layers:
- The *basal layer* is a single row of immature cells with large nuclei and a small amount of cytoplasm. Active mitosis occurs in this layer.
- The *parabasal layer* includes two to four rows of immature cells that have normal mitotic figures and provide the replacement cells for the overlying epithelium.
- The *intermediate layer* includes four to six rows of cells with large amounts of cytoplasm in a polyhedral shape separated by an intercellular space.
- The *superficial layer* includes five to eight rows of flattened cells with small uniform nuclei and a cytoplasm filled with glycogen. These cells are no longer maturing and readily exfoliate.
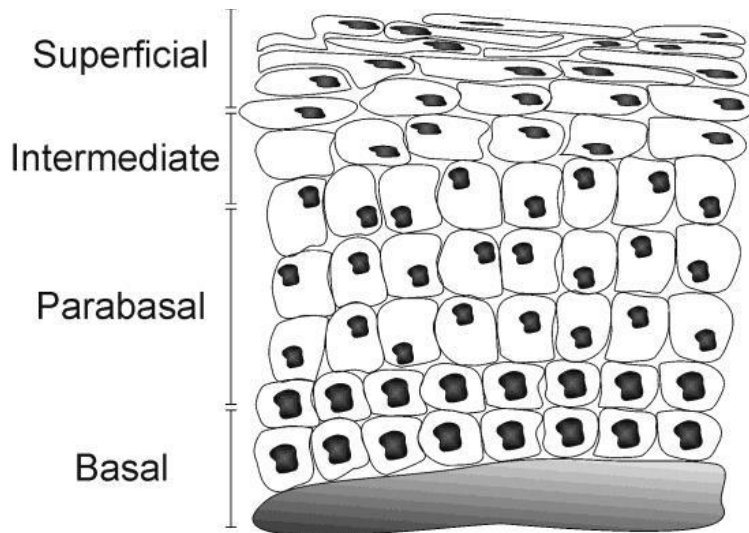
Figure 3.3-1 Cervical epithelial layers

Simple columnar epithelium lines the endocervix. The cells of this type of epithelium are much taller than they are wide and consist a single layer. Their apical surfaces may have cilia or microvilli, and they are specialized for secretion and absorption.
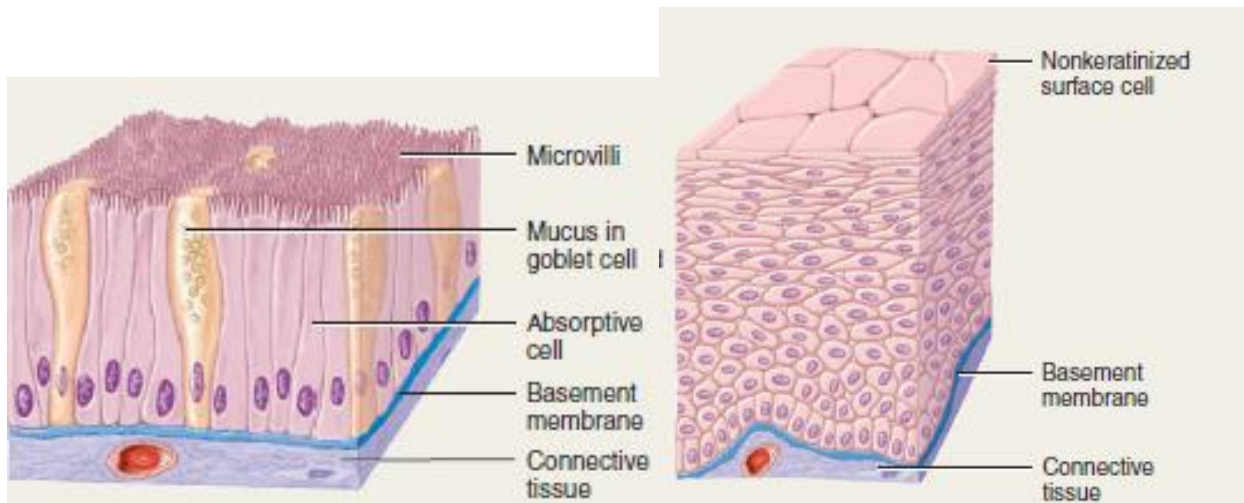
Figure 3.3-2 (left) Nonciliated simple columnar epithelium. (right) Nonkeratinized stratified squamous epithelium

3.4 Squamocolumnar Junction - Transformation Zone

The squamocolumnar junction (SCJ) is defined as the area where the squamous epithelium of the ectocervix and the columnar epithelium of the endocervix meet. This junction is visible through a colposcope and is the most common primary site within the cervix.

The SCJ rarely remains restricted to the external os. Instead it is a dynamic point that changes in response to puberty, pregnancy, menopause and hormonal stimulation. In neonates, the SCJ is located on the ectocervix. Upon entering puberty, due to hormonal influence, and during pregnancy, the columnar epithelium extends outwards over the ectocervix as the cervix everts. Hence, this also causes the squamocolumnar junction to move outwards onto the vaginal portion of the cervix, where it is exposed to the acidic vaginal environment. The exposed columnar epithelium can undergo physiological metaplasia and change to tougher metaplastic squamous epithelium in days or weeks, which when mature is very similar to the original squamous epithelium. The new squamocolumnar junction is therefore internal to the original squamocolumnar junction, and the zone of unstable epithelium between the two junctions is called the transformation zone of the cervix. After menopause, the uterine structures involute and the functional squamocolumnar junction moves into the endocervical canal.
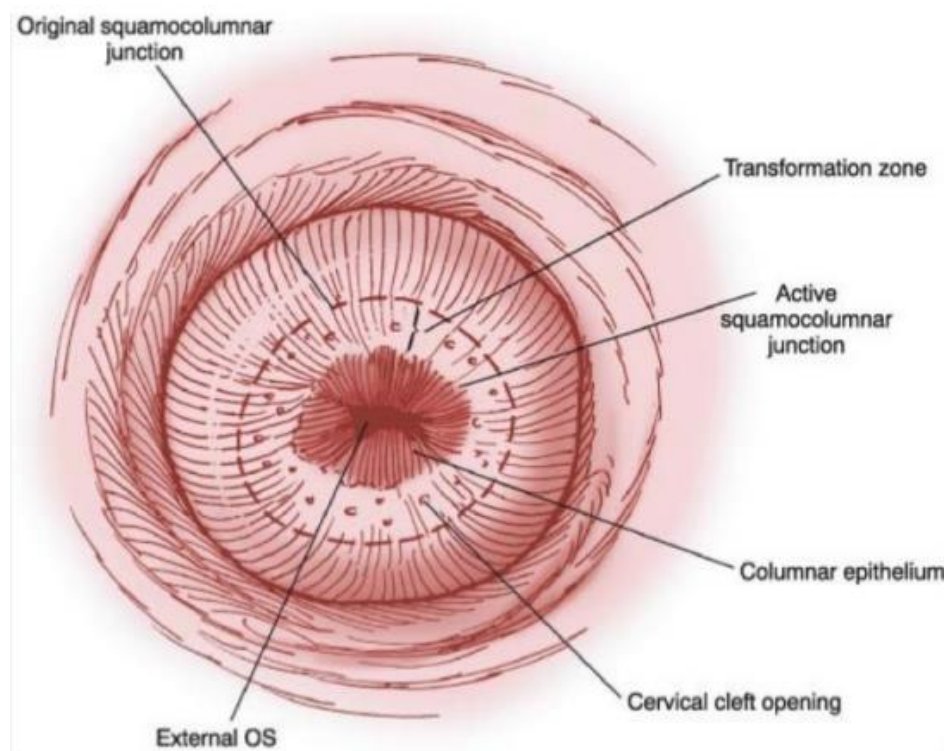
Figure 3.4-1 Original and active squamocolumnar junction

3.5 Pre-cancerous stages of the epithelium

As indicated in the introduction, cervical cancer arises as the end-point of a series of stages, which begin with a sexually transmitted high risk HPV virus infection of the cervical epithelium.
It is important to understand that HPV does not infect all regions of the female genital tract at the same frequency. It seems that the cervical transformation zone is of particular risk to HPV

carcinogenicity, since at this site, there are continuous metaplastic changes. The greatest risk of HPV infection coincides with greatest metaplastic activity.

HPV virus, like any virus, cannot multiply itself; it penetrates the cells and exploits their genetic mechanism in order to multiply. If, for any reason, the defensive mechanism of the body is suppressed, the infection evolves to inflammation. At this time, the virus begins to multiply uncontrollably inside the cells. New HPV infected cells are generated through mitosis. The function and morphology of the squamous epithelium cells is altered causing precancerous lesions to occur.

When the inflammation firstly develops, it is confined at the layers of the epithelium hence the term Cervical Intraepithelial Neoplasia. The proportion of the thickness of the epithelium showing mature and differentiated cells is used for grading CIN. Abnormal nuclei in superficial or intermediate cells indicate a low-grade CIN, whereas abnormality in nuclei of parabasal and basal cells indicates high-grade CIN. High grade CIN are likely to have a greater proportion of the thickness of epithelium composed of undifferentiated cells, with only a narrow layer of mature, differentiated cells on the surface.

In CIN 1 there is good maturation with minimal nuclear abnormalities and few mitotic figures. Undifferentiated cells are confined to the deeper layers (lower third) of the epithelium. Mitotic figures are present, but not very numerous.
CIN 2 is characterized by dysplastic cellular changes mostly restricted to the lower half or the lower two-thirds of the epithelium, with more marked nuclear abnormalities than in CIN 1. Mitotic figures may be seen throughout the lower half of the epithelium.
In CIN 3, differentiation and stratification may be totally absent or present only in the superficial quarter of the epithelium with numerous mitotic figures. Nuclear abnormalities extend throughout the thickness of the epithelium. Many mitotic figures have abnormal forms.

If the neoplastic process described above continues uninterrupted, the early low-grade lesions may eventually involve the full thickness of the epithelium. Subsequently the disease may traverse the basement membrane and become invasive cancer, extending to surrounding tissues and organs.

Normal   CIN I   CIN II   CIN III
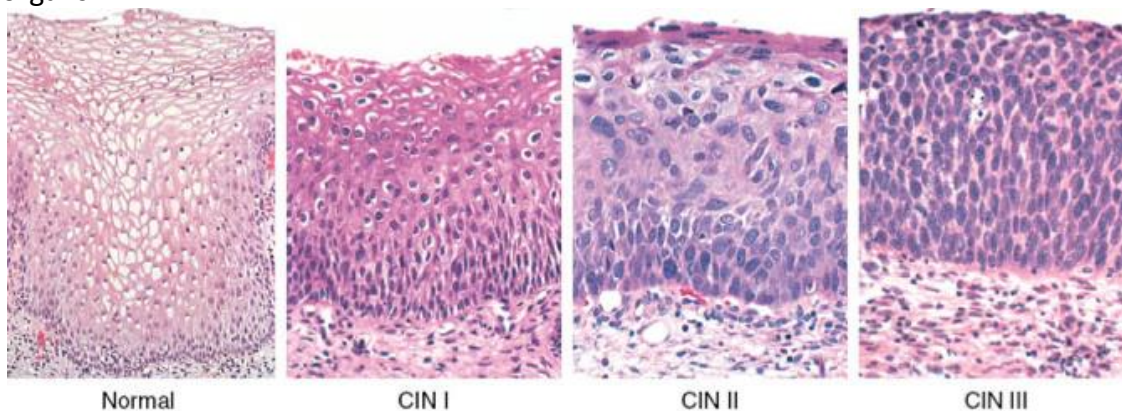
Figure 3.5-1 Cervical Intraepithelial Neoplasia Stages

4 Physics Model

4.1 Light

Light is electromagnetic radiation (EMR), within a certain portion of the electromagnetic field, directly depended from the properties of the light source emitting the radiation. The term visible light, refers to the part of the electromagnetic radiation that is visible to the human eye and to common sensor, such as commercially available CCD and CMOS, made to emulate the behavior of the human eye. Visible light is usually defined as having wavelengths between the range of 400 to 700 nanometers, bounded by infrared for longer wavelengths and the ultraviolet portion for shorter wavelengths. The respectful frequency is roughly at 430-450 THz.
Primary properties of visible light are intensity, propagation direction, frequency or wavelength, polarization. Its speed in a vacuum, 299,792,458 meters per second, is one of the fundamental constants of nature and the fastest moving object. Visible light, as with all types of electromagnetic radiation (EMR), is experimentally found to always move at this speed in vacuum.

Light exhibits a unique property known as wave-particle duality. It interacts with matter through tiny "packets", called photons or quanta, exhibiting properties of small particles, while being transmitted in vacuum exhibiting properties of waves. The study of light and the interaction of light and matter is an entire and important research area in modern physics science, known as optics.

The behavior of EMR depends on its wavelength. The energy transmitted in each quantum depends on the wavelength it is emitted from. This photonic energy cause electronic excitations which lead to changes in the bonding or chemistry of the molecules, accordingly on the amount of this energy.

4.2 Absorption

Absorption of electromagnetic radiation is the way in which the energy of a photon is taken up by matter, typically the electrons of an atom. These electrons are loosely bonded with atoms and tend to vibrate. When light with frequency that resonates to the frequency in which electrons vibrate, incidents upon an atom, then the electrons of that atom will become excited and set into higher vibrational motion. Energy wise, electromagnetic energy carried by light is transmuted into kinetic energy of the electrons, which consists the thermal energy of matter. Absorption can be either linear, where the volume of absorption does not depend on the intensity of the electromagnetic wave, or nonlinear, where the transparency of the medium changes accordingly to the intensity. Techniques and methodologies used to quantify absorption depend on the field on study and the choice of a given practitioner. The absorbance of a matter quantifies how much of the incident light is absorbed by it instead of being reflected or refracted. Through the Beer-Lambert law, this quantity can be related to other properties of matter. Precise measurements of the absorbance at many wavelengths allow the identification of a substance via spectroscopy,

given standard known illumination, by measuring the intensity of the light after interaction with the substance.

4.3 Reflection

Reflection is the change in direction of the light when at the interface between two different media, leading to partial or total return of the electromagnetic energy to the medium from which it originated.

Refraction can be either specular or diffuse. Specular reflection is mirror-like reflection from a surface, in which light from a single incoming direction is reflected into a single outgoing direction. According to the law of reflection, the angle at which the wave is incident on the surface equals to the angle at which it is reflected. Diffuse reflection is the reflection of light from a surface, such that an incident ray of light is reflected at many angles.
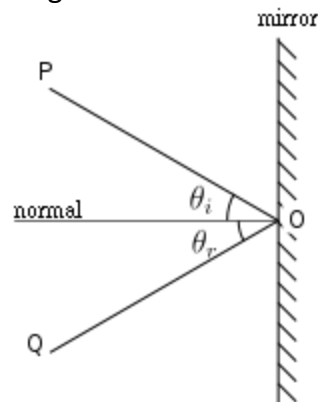
Figure 4.3-1 Diagram of specular reflection

The laws which govern reflection are as follows:

1. The incident ray, the reflected ray and the normal to the reflection surface at the point of the incidence lie in the same plane.
2. The angle which the incident ray makes with the normal is equal to the angle which the reflected ray makes to the same normal.
3. The reflected ray and the incident ray are on the opposite sides of the normal.

These three laws can all be derived from the Fresnel equations.
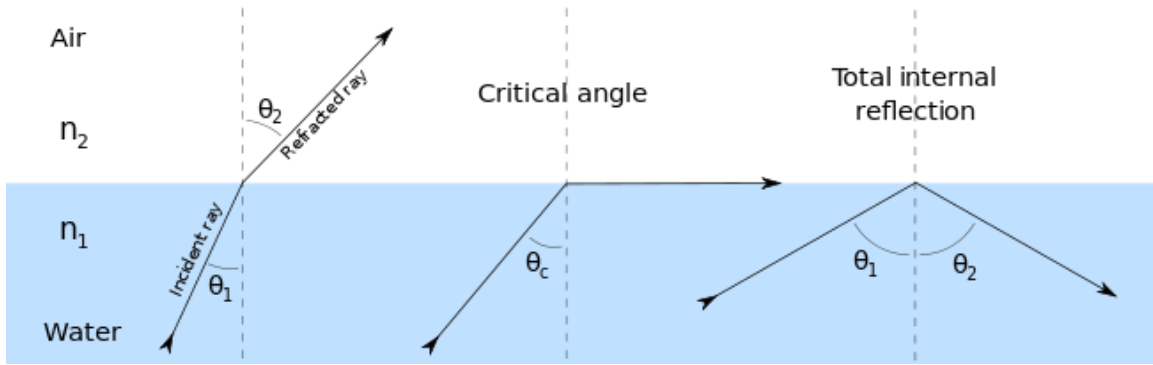
Figure 4.3-2 Refraction of light at the interface between two media

When light strikes the surface of a non-metallic material it bounces off in all directions due to multiple reflections by the microscopic irregularities inside the material and by its surface. This phenomenon is called diffuse reflection and is often referred as scattering. The exact form of the reflection depends on the structure of the material. One common model for diffuse reflection is Lambertian reflectance, in which the light is reflected with equal luminance in all directions, as defined by Lambert's cosine law. The light sent to our eyes by most of the objects we see is due to diffuse reflection from their surface, so that this is our primary mechanism of physical observation.

4.4 Scattering

Scattering is a general physical process where some forms of radiation are forced to deviate from a straight trajectory by one or more paths due to localized irregularities in the medium through which they pass. In conventional use, this also includes deviation of reflected radiation from the angle predicted by the laws of reflection. When these irregularities are considered to be random and dense enough that their individual effects average out, this kind of scattered reflection is commonly referred to as diffuse reflection.
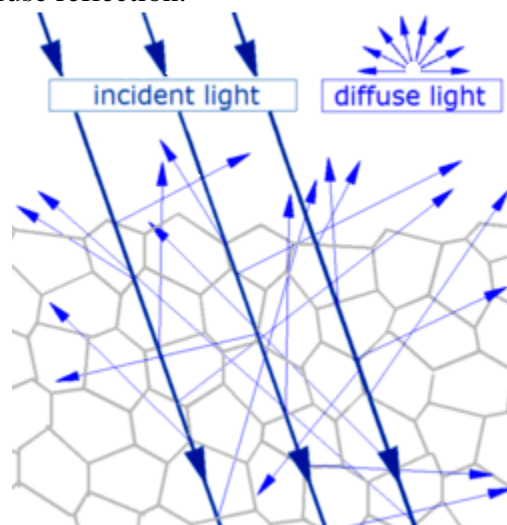
Figure 4.4-1 Mechanisms of diffuse reflection

Scattering of light depends on the wavelength or frequency of the light being scattered, as well as the properties of the medium scattering light. Matter is composed of discrete electrical charges. On the other hand, light is an oscillating EM field – excites charges, which radiate EM waves. These radiated EM waves are scattered waves, excited by a source external to the scatterer. The superposition of incident and scattered EM waves is what is observed. This interaction can reveal important information about the structure and dynamics of the material being examined. A study of the scattered light intensity as a function of scattering angle gives information about the structure, spatial configuration, or morphology of the scattering medium. Scattering is dependent on the wavelength of the incident radiation, the size of the scattering particle and the complex refractive index, which describe the particle optical properties relative to the surrounding medium.

The size of the scattering particle is calculated as:

$$x = \frac{2\pi r}{\lambda}$$

Where
- r is the radius of the spherical particle
- λ is the wavelength of the incident light
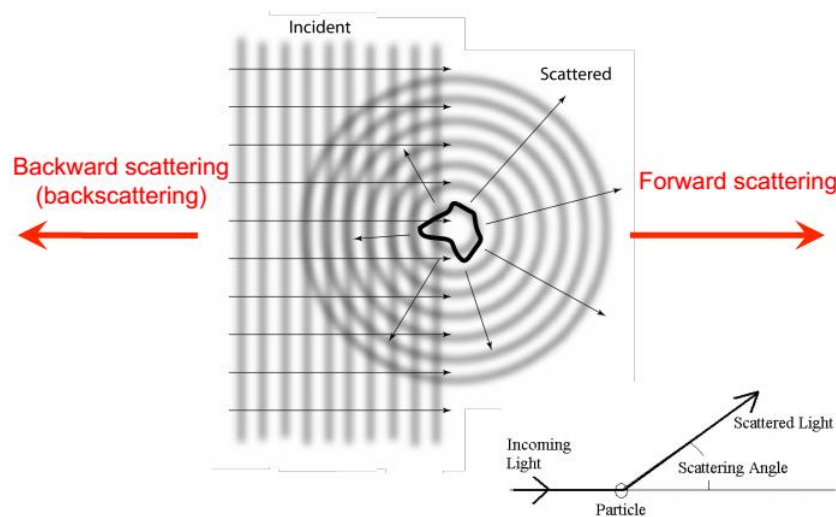
Figure 4.4-2 Scattering geometry

There are several types of scattering:
- Elastic scattering, where the wavelength (frequency) of the scattered light is the same as the incident light (Rayleigh(where x<<1) and Mie scattering (where x ~=1))
- Inelastic Scattering, where the emitted radiation has a wavelength different from that of the incident radiation(Raman scattering, fluorescence)
- Quasi-elastic scattering, where the wavelength (frequency)of the scattered light shifts (e.g., in moving matter due to Doppler effects)

- Single scattering, where photons scattered only once. It prevails in optically thin media (τ<< 1), since photons have a high probability of exiting the medium (e.g., a thin cloud) before being scattered again and is also favored in strongly absorbing media (ω<< 1)
- Multiple scattering, which prevails in optically thick, strongly scattering and non-absorbing media.

Scattering by particles similar to, or larger than, the wavelength of light is typically treated by the Mie theory, the discrete dipole approximation and other computational techniques. Rayleigh scattering applies to particles that are small with respect to wavelengths of light, and that are optically "soft" (i.e. with a refractive index close to 1). On the other hand, Anomalous Diffraction Theory applies to optically soft but larger particles.

4.5 Mie scattering

The Mie scattering theory is named after its developer, German physicist Gustav Mie. It refers to the scattering of light by particles with size comparable or larger than the wavelength of the incident light. Because Mie scattering is hardly wavelength dependent, scattered light looks white or light bluish, depending on the size of the scattering particles. In Mie scattering, the direction of the scattered light peaks forward, as is shown in figure below.
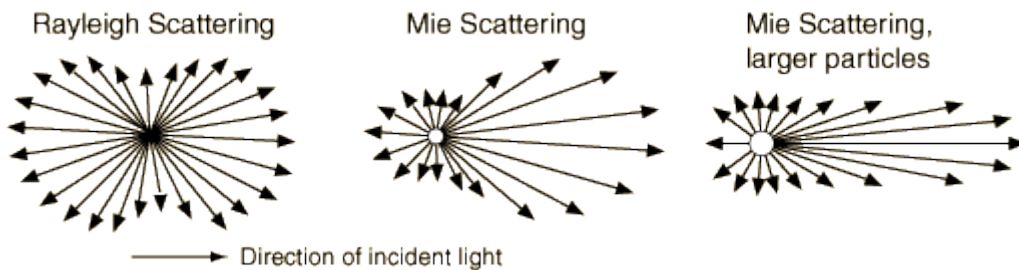
Figure 4.5-1 Scattering paterns

4.6 Rayleigh scattering

Rayleigh scattering, named after the British physicist Lord Rayleigh (John William Strutt), is the dominantly elastic scattering of radiation by particles much smaller than the wavelength of the radiation. The particles may be individual atoms or molecules. Rayleigh scattering results from the electric polarizability of the particles. The oscillating electric field of a light wave acts on the charges within a particle, causing them to move at the same frequency. The particle therefore becomes a small radiating dipole whose radiation we see as scattered light. This practically means that Rayleigh scattering becomes more dominant in wavelengths with higher energy, such as blue compared to red, meaning that the scattered intensity is dependent to the light wavelength. In fact it is proportional to$(\frac{1}{\lambda^4})$. The amount of Rayleigh scattering magnitude is not constant but varies upon the angle through which scattered light is emitted, called scattering angle.

The formula of Rayleigh scattering is:

$$I = Io \frac{1 + cos^2(\theta)}{2R^2} (\frac{2\pi}{\lambda})^4 (\frac{n^2 - 1}{n^2 + 2})^2 (\frac{d}{2})^6 \qquad (2.7)$$

Where
- I_0 is the intensity of the incident radiation,
- R the distance to the particle,
- θ the scattering angle,
- λ the wavelength of the incident light,
- n the refractive index of the particle and
- d the diameter of the particle.
  The $cos^2(\theta)$ shows that the radiation is emitted uniformly in all directions.

4.7   Acetowhitening effect

Measurements of the visible spectrum of the scattering coefficient of the particles indicate that the scattering coefficient of the particles may exhibit definite wavelength dependency. In Figure 4.7-1, it is obvious that Mie scattering is less dependent on the wavelength if compared to Rayleigh scattering. If the light incident on large particles is white in color, the particles are capable to scatter all wavelengths of white light equally. While, in the other hand, smaller particles tend to scatter the shorter wavelengths of white light such as violet, blue and green more effectively than the longer orange, yellow and red wavelengths.
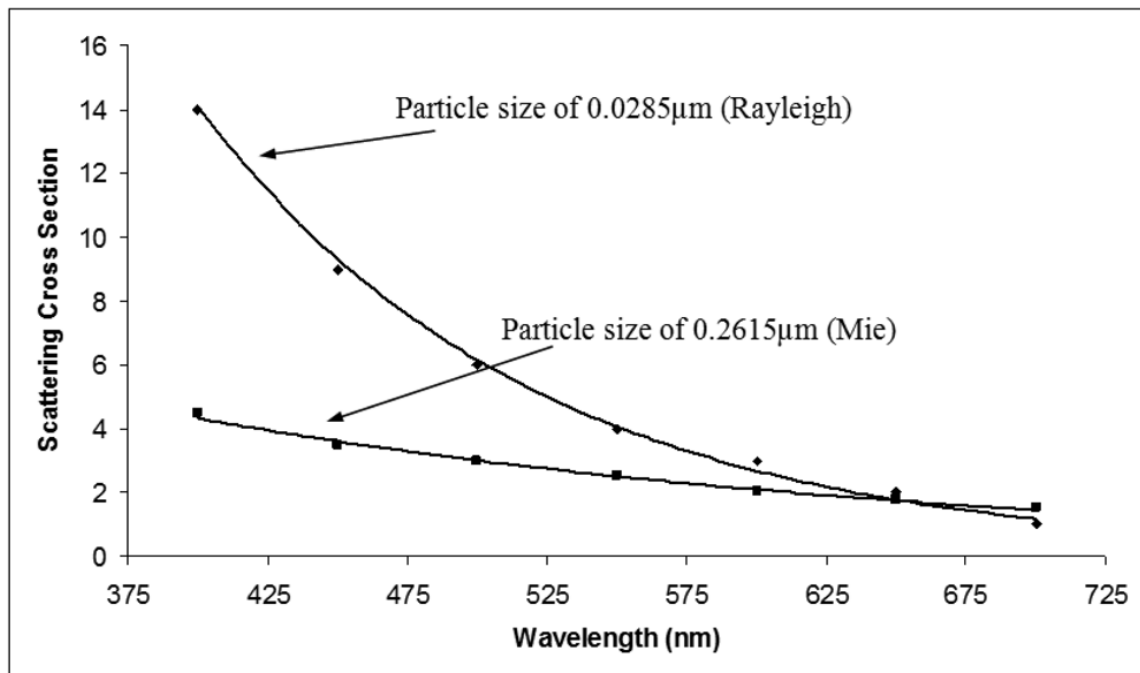
Figure 4.7-1 Scattering cross section of both Rayleigh and Mie vs wavelength for specific size of particles.

The acetowhitening phenomenon, interferes with the normal functionality of a given cell, in altering the way it interacts with light, as far as scattering is concerned, but retaining its behavior as far as absorption and reflection is concerned. In the scope of the current thesis, we investigate the alterations of light-tissue interaction, focusing in the scattering effect to deduct an objective parameter of the AW effect.

Prior research work [27] has shown that backscattering (scattering in large angles), recorded from the acetowhitening phenomenon, is strongly wavelength dependent, which implies that backscattering mainly follows Rayleigh law. This fact strongly supports that the main AW backscatterers are protein aggregates of the size of the wavelength of the optical radiation. This finding provides a valuable mean for discriminating the AW effect from other structural features such as keratin deposits which seem to follow the Mie scattering law, as being larger structures. We exploit these tissue-physics model to define physical parameters that are sensitive to the previously discussed scattering changes.

A first parametrical attempt to quantify the scattering changes of the tissue was

$$\frac{B-G}{B+G}$$

as a parameter that expresses the dominance of the Rayleigh scattering mechanism. If B>G then Rayleigh is dominant. This parameter was quickly found to be experimentally inadequate due to the nature of the denominator. The slight differences in Rayleigh are not easy to be captured by this parameter, since higher scattering effects in the blue channel, as are expected by Rayleigh law, would lead to greater denominator and smaller parameter.

We therefore define a new parameter:

$$\frac{B-G}{255-G}$$

as a parameter that expresses the dominance of the Rayleigh scattering mechanism. If B>G then Rayleigh is dominant, where 255-G expresses the general scattering intensity at the same wavelength. If there is high scattering in the green portion of the spectrum then the denominator will be reduced and the parameter will be increased.

4.8   Light recorded in a sensor

An image processing algorithm evaluates the pixel intensity recorded in a single frame. This arises some fundamental issues in extracting information from an image. The information recorded in an image is a convolution of pieces of information from different sources and not simply from the object in interest.

Light could be precisely characterized by giving the distribution of power of the light at each wavelength in the visible spectrum, known as the spectral power distribution (SPD).It contains all the basic physical data about light and serves as the starting point for quantitative analyses of

color. SPD power and morphology can be measured by a spectrophotometer. The SPD of optical radiation from an illuminated surface is the product of the percent reflected by the surface, the SPD of the light which falls onto the surface and the SPD recorded by a given sensor.

This means that in a given imaging setup there are three main sources that have a direct impact on the intensity recorded. These are

- The light source
- The imaging sensor
- The spectral response of the targeted object

Each light source, whether it is a LED or a halogen lamp, or even the sun itself, has different SPDs, emitting different intensity per nanometer.

An imaging sensor, whether it is a monochrome sensor or, like in our case, a color sensor, is based on the optical characteristics of a light sensitive material as well as specialized optics and lenses. A color sensor has three different optics leading to three different spectral sensitivities, one for each camera channel. Lighting conditions that exceed the sensitivity of a given sensor, lead to saturation.

The spectral response of a given object is characteristic of the materials consisting the object. The spectrum reflected from an object is formed by direct interaction of a photon and the molecules of the material.

Figure 4.8-1 The reflected SPD by a given surface under different illumination
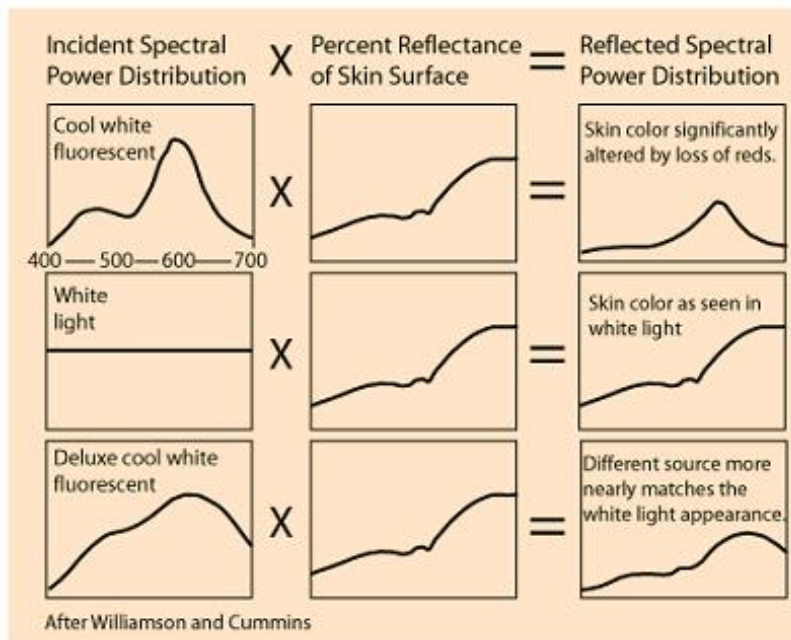
This leads to the conclusion that in an algorithm of real time implementation purposes, it is imperative to compensate for changes in the lighting conditions and in making sure that the dynamic range of the sensor used, is not led to saturation.

5 Algorithm implementation

5.1 Dataset from previous clinical studies

The data used in the current thesis were collected during the second clinical trial of DySIS™ that took place in the Netherlands. DySIS™ and biopsy results for 275 patients were collected. Careful examination of the set was needed, in order to exclude outliers, such as cases with bleeding tissue, glare artifacts, foam and excessive mucus.
In order to train and validate our algorithm, two different sets were created.

Training Set
20 cases were selected as part of the training set. Half of those cases were confirmed CIN3 by biopsy and the other half were confirmed CIN1.

Validation set
70 cases were selected as part of the validation set. Training set was not included in the validation set, in order to avoid bias. Of those 70 cases, 58 were confirmed normal- CIN1, 12 patients were confirmed CIN2 and 10 were confirmed CIN3-HG.

A very essential hypothesis, regarding CIN2, was also made; CIN2 has a higher probability in regressing to CIN1, as opposed to CIN3 regressing back to CIN2. Moreover, the aim of this thesis is the detection of irreversible high grade lesions. With these in mind, it was preferred to regard CIN II as low grade lesions.

5.2 Acetowhitening detection algorithm

As mention in section 2.3, DySIS™ calculates the diffuse-reflectance curves for every pixel of the image. The curves represent the development of the AW over the course of time. Based on previous work, a crucial observation was made, that inspired this method.

Approximately a minute after the application of acetic acid, the AW phenomenon reaches its peak and soon after exhibits a decline. The decline rate varies from to case to case, though there is a specific pattern distinguishing high from low grade lesions, with high grade showing a tendency to persist for a longer period of time than low grades. After approximately a minute, it is safe to assume that the phenomenon that persists indicates a high grade lesion.
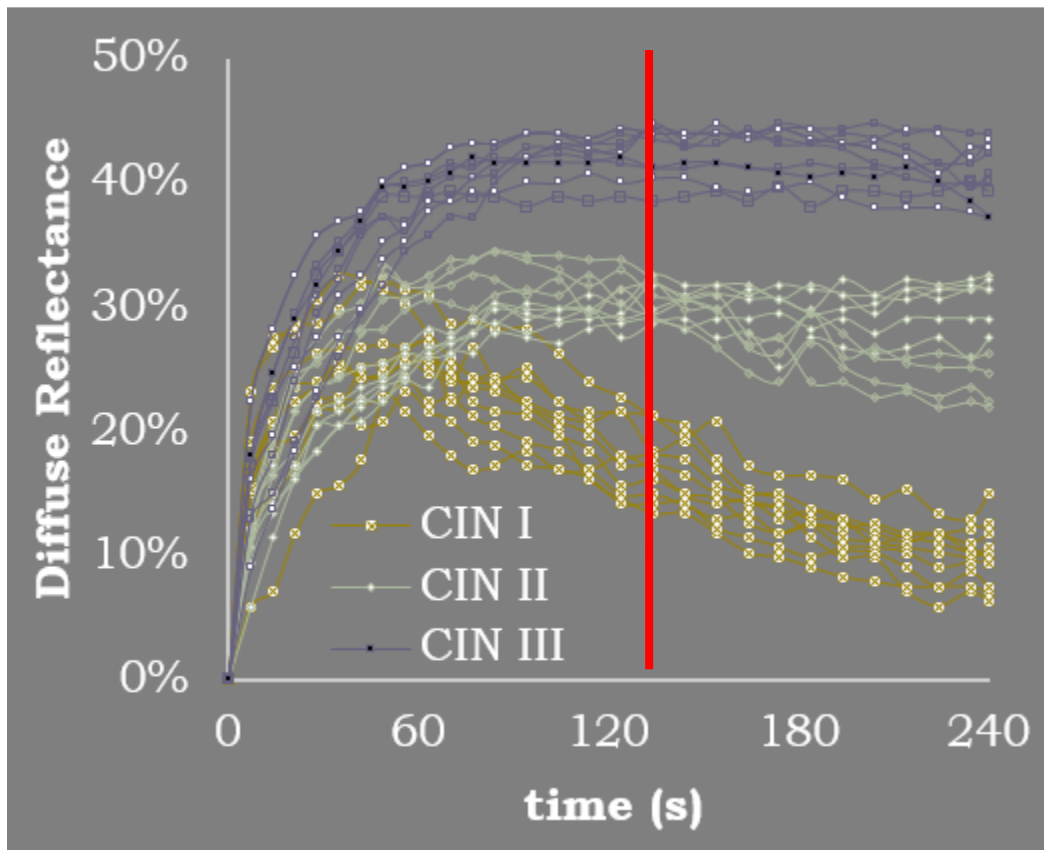
Figure 5.2-1 Diffuse reflectance intensity curves over time, as captured by DySIS™

The goal of the proposed algorithm is the extraction of features of diagnostics importance from a single frame in order to detect and grade potential lesions. The algorithm described below can be applied independently to each frame of a given case. For every step of the algorithm, we also present intermediate results from a selected case.

- The algorithm takes as input a single frame. This method is implemented simultaneously for frames at 0 and 144 seconds. Frame 0s is loaded in order to be used as a reference for the training and calibration of the algorithm. Frame 144s is selected due to the behavior of the AW phenomenon. We will refer to these as "img0" and "img144" respectively. Both images are in RGB color space.

- The following ratio is used for normalization :

$$normalized(i) = \frac{blue(i) - green(i)}{255 - green(i)}$$

The ratio is applied on both frames and is calculated for every pixel. A new, grayscale image is returned, with values between 0 and 1, inclusive.

- Since we are interested in keeping information related only to the AW phenomenon, a threshold needs to be applied. Using a threshold, we are able to remove all the information that appears at img0 and at the same time maintain only acetowhitening regions at img144. Therefore, anything below the selected threshold is removed, leaving intact all pixels with values greater than the threshold.

$$cutoff_{normalized(i)} = ((normalized(i) < th) == 0)$$

- We then construct a pseudomap based on the values of the final image. The pseudomap is comprised of three colors;blue, green and yelllow. The pseudomap is then overlaid on the initial RGB images, thus indicating areas where abnormal cells exist.

```
        ┌─────────────┐
        │    start    │
        └─────────────┘
               │
               ▼
   ┌───────────────────────┐
   │  load frames from 0 sec│
   │      and 144 sec       │
   └───────────────────────┘
               │
               ▼
```

calculate

$$normalized(i) = \frac{blue(i) - green(i)}{255 - green(i)}$$

for every pixel i, on both frames

cut off image(i)<th, where th a manually selected threshold

overlay pseudocolor map on final image0 and image144

```
        ┌─────────────┐
        │     end     │
        └─────────────┘
```
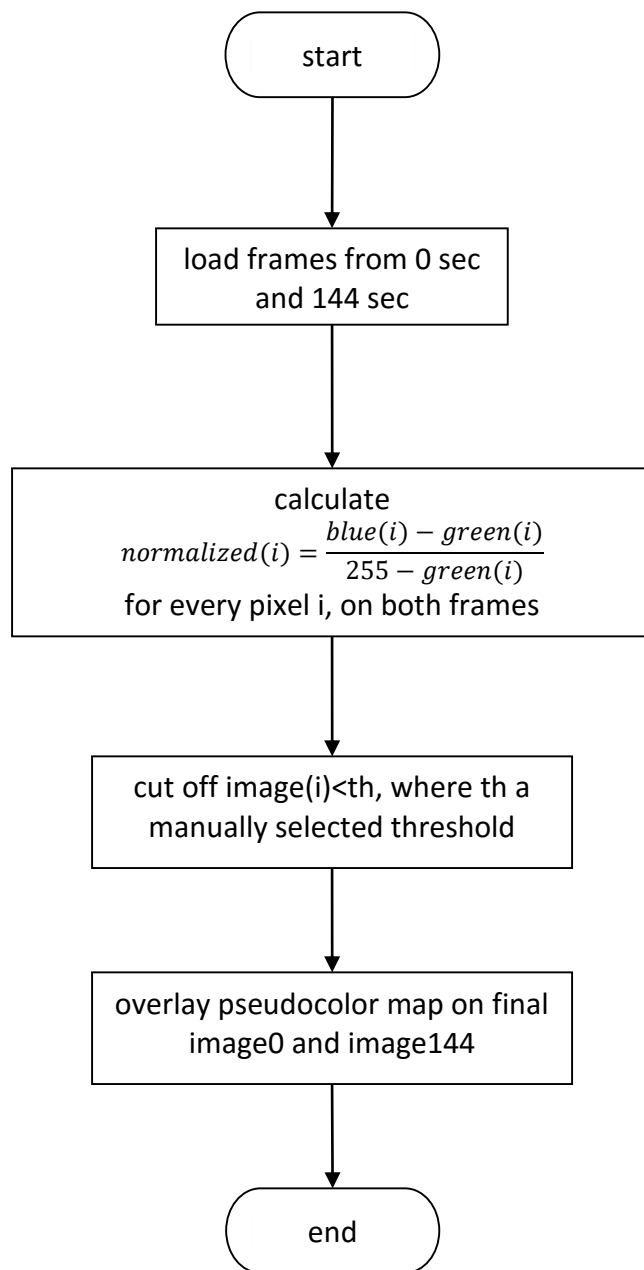
Figure 5.2-2 Flow chart of Physics based model Algorithm

A confirmed high grade case, part of the training set, is used in order to visualize the intermediate steps. As mentioned earlier, we use frames 0 and 144. Firstly, we present the RGB images:
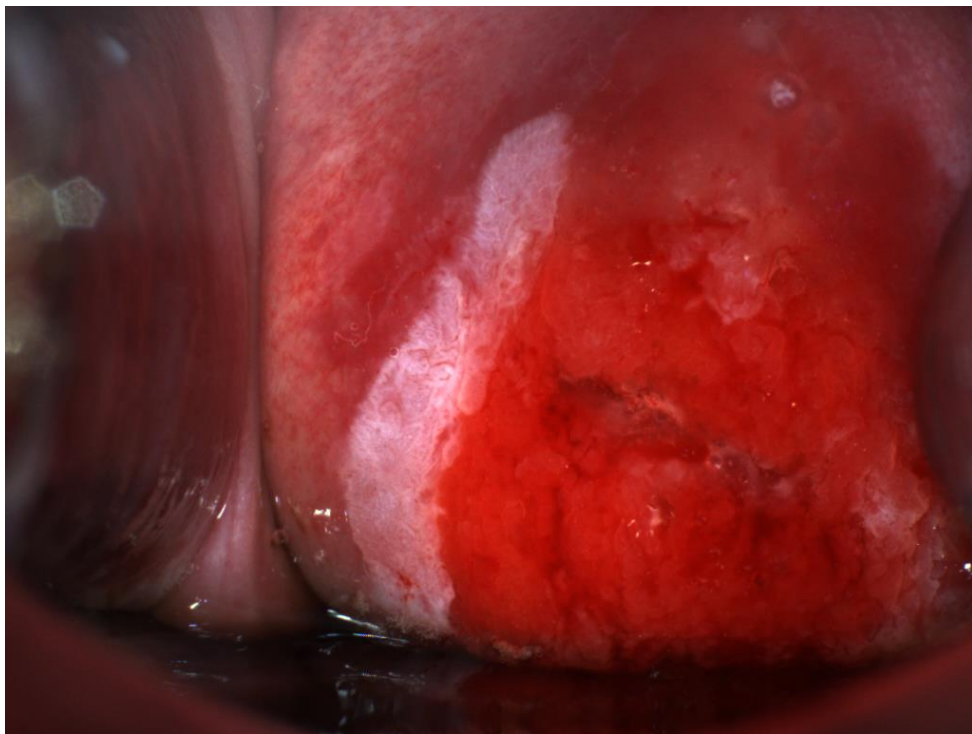
Figure 5.2-3 Captured frames from confirmed high grade case (above) frame at 0 seconds before application of acetic acid (below) frame at 144 seconds after the application of acetic acid

We then apply the ratio on the RGB images:
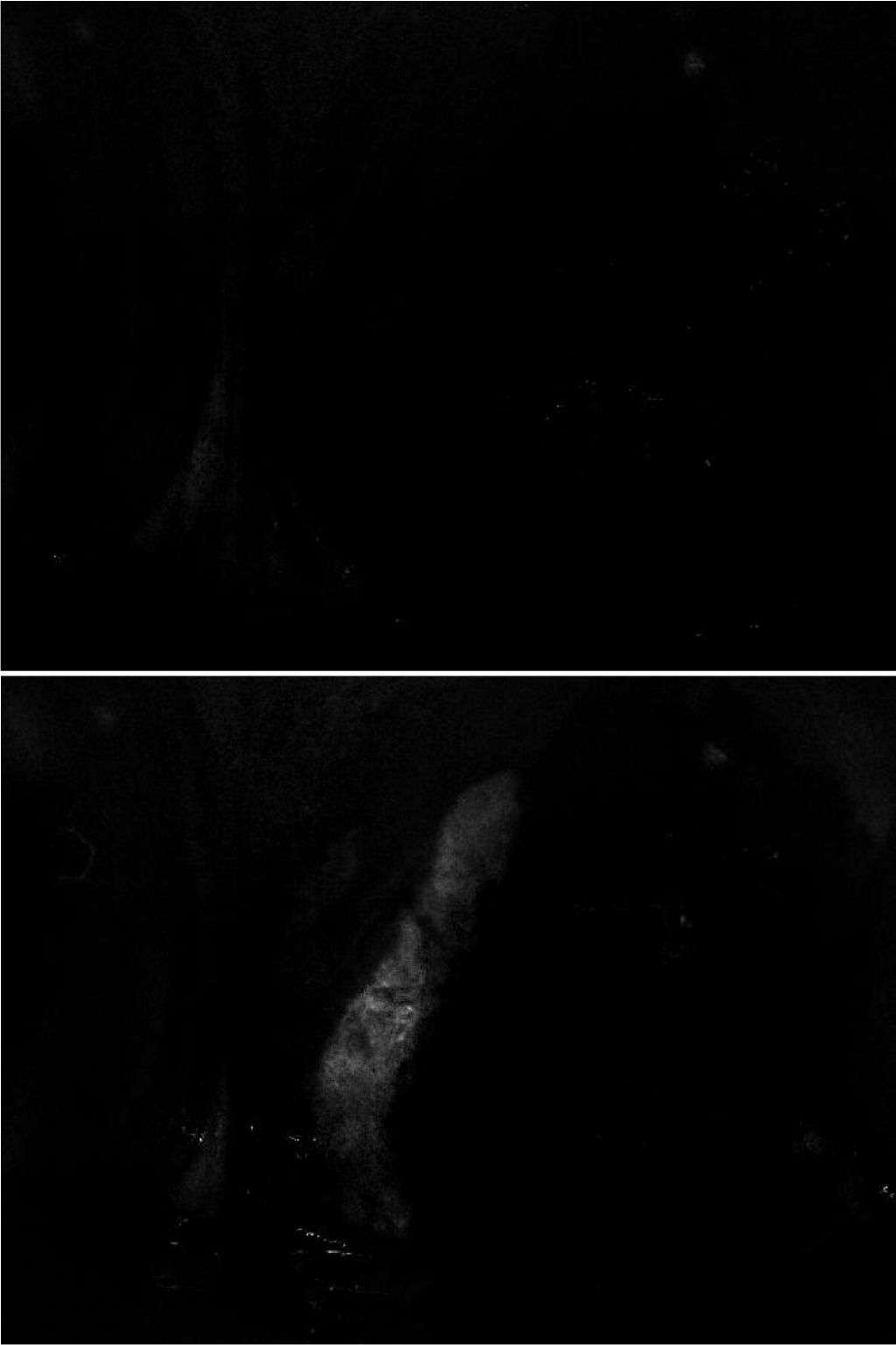
Figure 5.2-4 Ratio encapsulating Rayleigh dominance applied in a confirmed high grade case (above) frame at 0 seconds before application of acetic acid (below) frame at 144 seconds after the application of acetic acid

Manual threshold was estimated at th = 0.15. Anything below th is cut off:
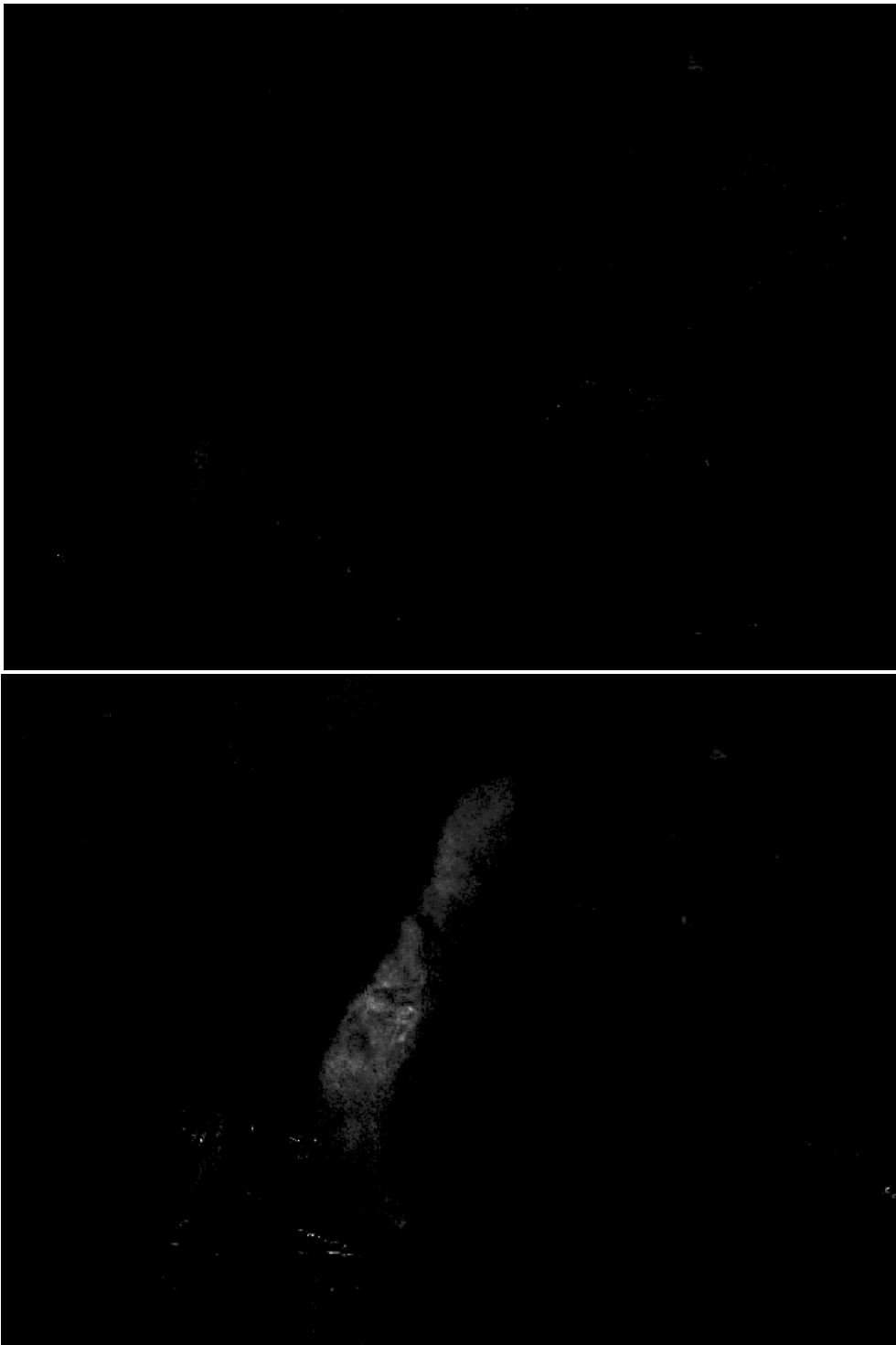
Figure 5.2-5 Ratio encapsulating Rayleigh dominance after thresholding manually, applied in a confirmed high grade case (above) frame at 0 seconds before application of acetic acid (below) frame at 144 seconds after the application of acetic acid

The pseudomap is constructed and overlaid on both RGB images:
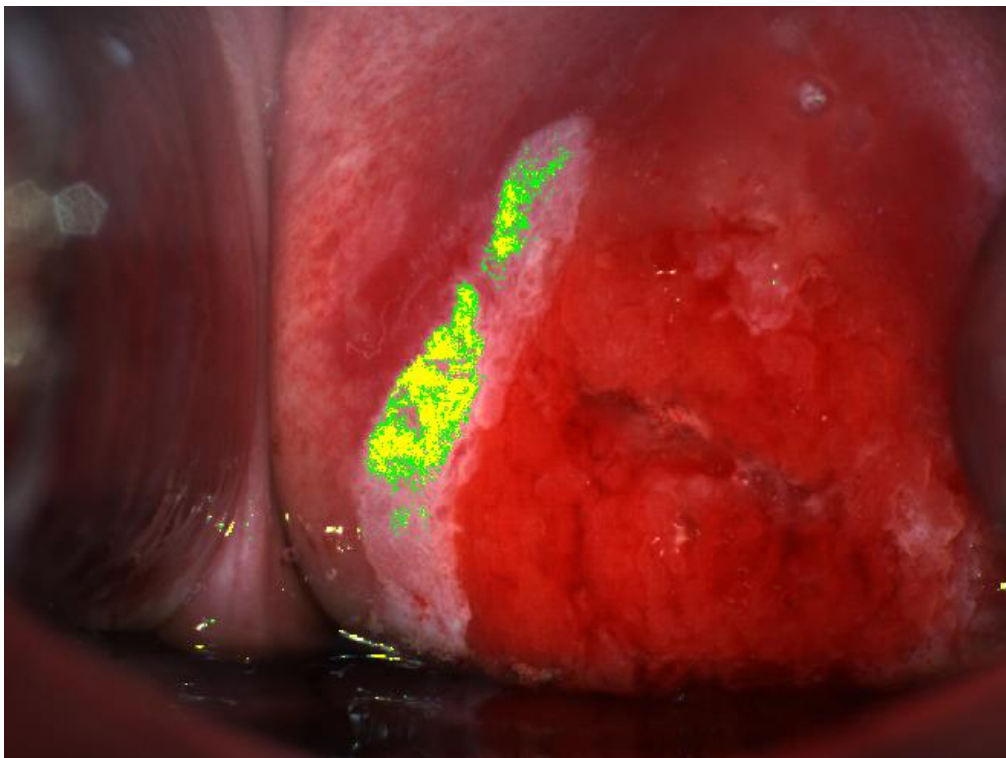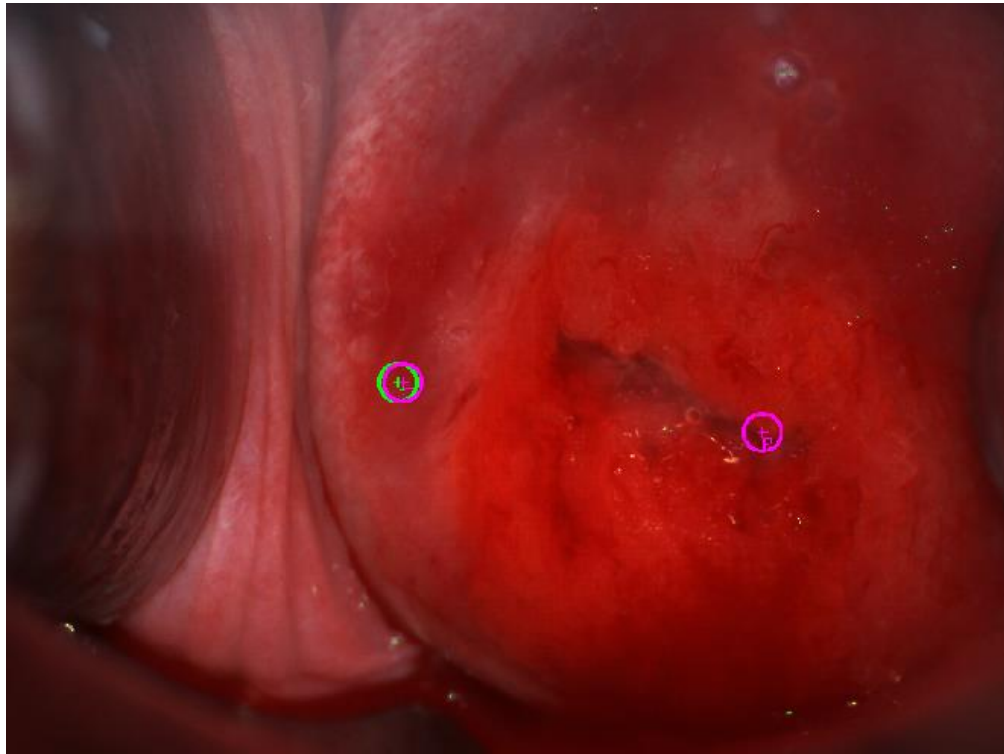
Figure 5.2-6 Captured frames, with overlaid pseudocolor map depicting intensified AW phenomenon, from confirmed high grade case (above) frame at 0 seconds before application of acetic acid (below) frame at 144 seconds after the application of acetic acid
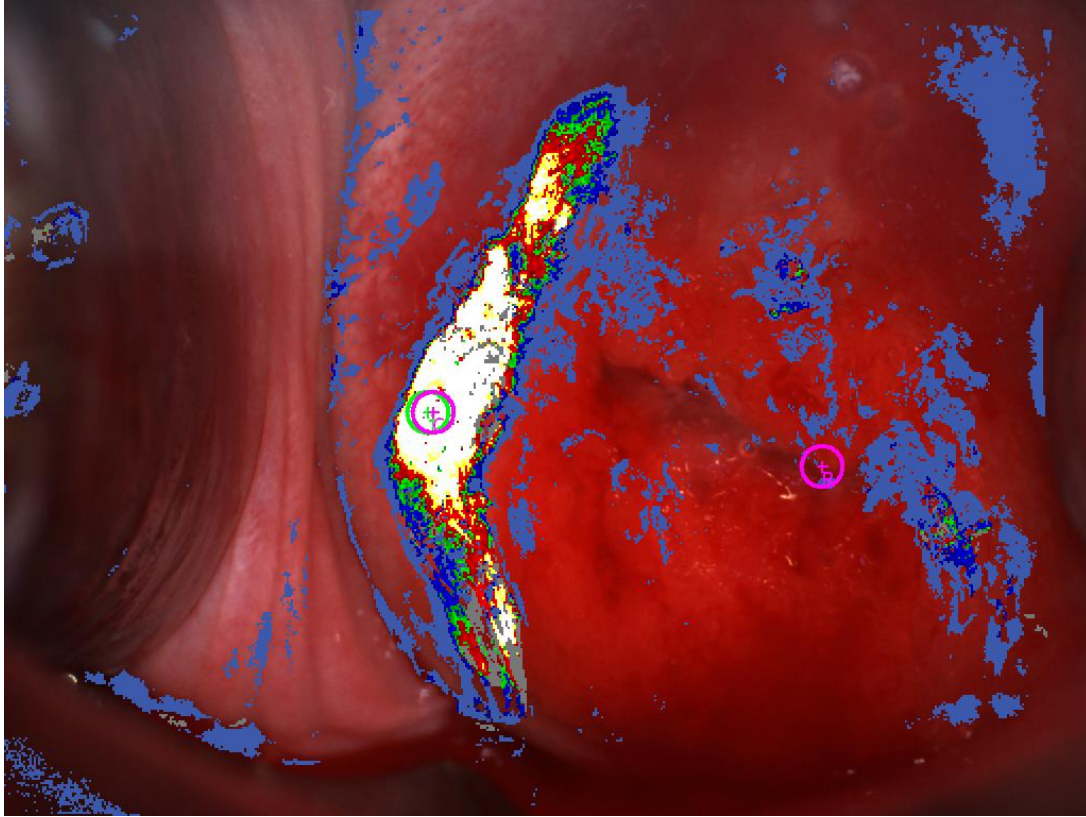
Figure 5.2-7 DySIS psedocolor map

As we can see in Figures 5.2-4 and 5.2-5, after applying a cut off threshold, a lot of unnecessary information is excluded. Frame 0 contains almost no information; any pixels left represent areas of glares. Frame 144 contains all the information associated with the AW phenomenon.

The pseudomap provides better visualization of the final results. As we can see there is no map overlaid on Frame 0; we have successfully eliminated all information not associated with the AW phenomenon. On the other hand, Frame 144 exhibits an intense pseudomap.

The algorithm is designed in a way that only high grade abnormalities will eventually appear. If we assess the RGB image of frame 144, as in conventional colposcopy, we can identify a greater area exhibiting the AW effect as opposed to the map of the proposed algorithm. On the other hand, the algorithm grades the intensity of the phenomenon indicating the severity of the lesion.

If we compare our map with the map of DySIS™, we can see consistency in identifying high grade lesions, where both pseudomaps properly grade the phenomenon and emphasize in high grade areas. At the same time, DySIS™, despite having knowledge of the evolution of the phenomenon, shows some artifacts from glares and the speculum.

5.3   Threshold Optimization

The need for optimization of the threshold selection is clear; manually selecting an appropriate threshold for every unknown case is neither effective, nor easy. Moreover, manually selecting a threshold does not ensure the algorithm's ability to be applied on a single frame without the use of a reference frame. Aiming to abolish the need for a reference frame, we then proceed to examine a different approach when it comes to automatically extracting an appropriate threshold for any given case.
In order to train the optimized technique that follows, a set of 20 cases is used, referred to as training set.

5.3.1   Light intensity median

Due to the fact that environmental lighting conditions are never the same during an examination, there is a direct impact on the light intensities recorder by the camera. This can lead to malfunctions of the algorithm, since it can misinterpret changes in lighting. For these reasons, we need a way out to compensate for these changes.

Both red and blue channels of the image are utilized for that purpose; red channel contains information about the reflective intensity of the tissue whereas blue channel contains information about the backscattering. We are only interested in extracting light intensity from image144, since it is the one containing information of AW.

The first step is to identify those areas in blue channel that are representative of normal tissue and have no alterations due to the acetic acid. Those areas appear red in the RGB color space and black in the blue channel. Therefore, in order to extract information about the normal areas of the tissue, we find all pixels with values between specific limits. Those limits were calculated after training the system as it will be described in the following section.

$$[x, y] = \text{find}(\text{blue} \geq 10 \,\&\, blue \leq 100)$$

The indices of the pixels selected are returned. We then access the same indices on the red channel and extract their values. We now have a set of values associated with the light intensity of the image. With the values at hand, we calculated the median. The median is chosen because it is less sensitive to outliers as opposed to the mean and is indicative to the volume of pixels representing red tissue and the intensity of the reflectance and backscattering recorded in that set of pixels.
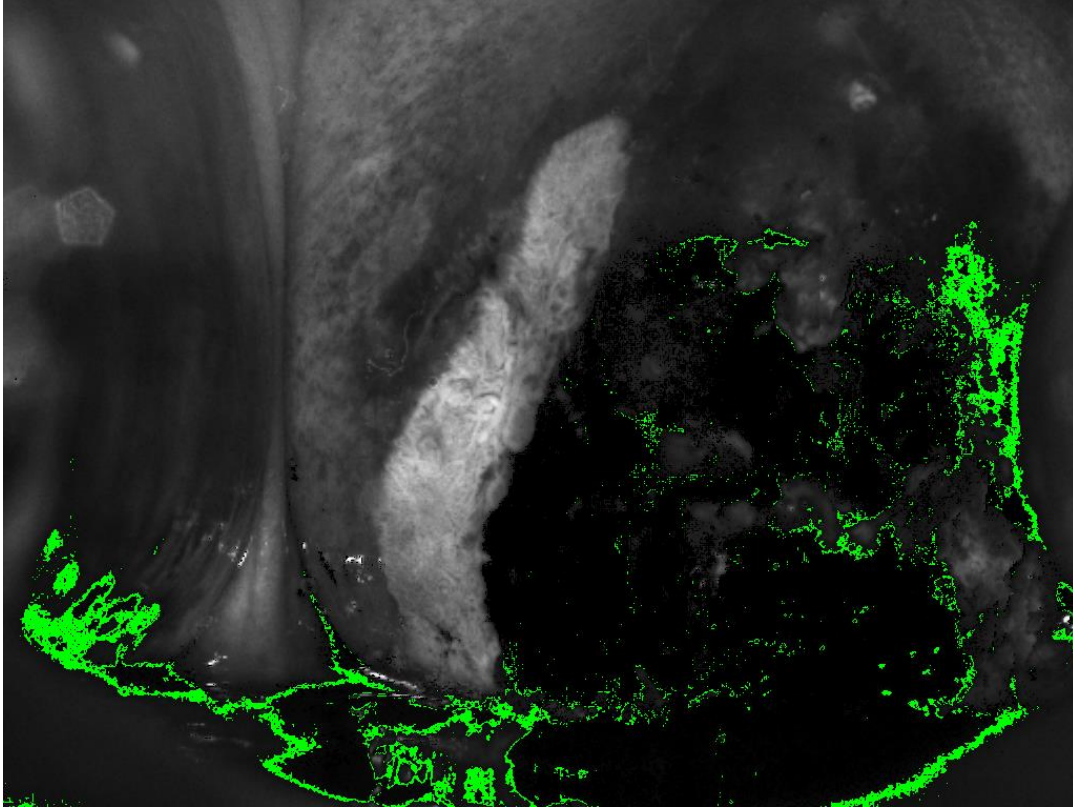
Figure 5.3-1 Pseudocoloring of the pixels selected to calculate the median for automatic thresholding

In Figure 5.3-1 we can see the areas used for the calculation of the median (colored green).The median for this specific case was 135. After solving the equation ... for th, the automatic threshold is th = 0.1136.

5.3.2 Spearman correlation coefficient

As previously noted, a metric was calculated in order to identify the reflectance of an unknown biological tissue. The reflectance of the image needs to be corrected in order to only perceive the intensity associated with the biological tissue.

For every single case of our training set, a cutoff threshold was calculated. Those thresholds were manually calculated, in a way that no information was kept at image0. At the same time, the photometry of every image was extracted. Basically, two sets of data were at hand; 20 thresholds and 20 luminance values, pair wise for each case.

The level of correlation between those datasets was then calculated. Correlation is a bivariate analysis that measures the strength of association between two variables. In our case, spearman correlation was used to examine whether our two datasets were associated and how. An important underlying assumption of spearman correlation is that the relationship between the two variables is described using a monotonic function. Moreover, one of Spearman's coefficient strengths is that it is less sensitive to strong outliers in the tails of the samples, as opposed to Pearson correlation.

A perfect spearman correlation lies between the values -1 and +1. A positive Spearman coefficient corresponds to an increasing monotonic relationship between variables X and Y, whereas a negative coefficient corresponds to a decreasing monotonic relationship. When X and Y are perfectly monotonically related, the Spearman correlation coefficient becomes +1/-1. Coefficient values above 0.6 suggest strong association between the variables.
Depending on whether the data have tied ranks or not, the appropriate formula is applied.
The formula for when there are no tied ranks is:

$$\rho = 1 - \frac{6 \sum d_i^2}{n(n^2 - 1)}$$

Where d_i = difference in paired ranks and n = number of cases.

The formula used when there are tied ranks is:

$$\rho = \frac{\sum_i (x_i - \bar{x})(y_i - \bar{y})}{\sqrt{\sum_i (x_i - \bar{x})^2 \sum_i (y_i - \bar{y})^2}}$$

Where i = paired score.

After applying spearman's correlation methodology, a coefficient is returned describing the level of correlation. This coefficient is equal to coef = -0.8749, indicating a strong, decreasing monotonic association between threshold and median.

Since we had no previous knowledge regarding the optimum range of values for the median calculation that, in conjunction with the thresholds, would yield a statistically sufficient Spearman coefficient, an exhaustive search is implemented. An initial range of values [10,100] for the median was selected. For every combination, spearman's correlation was calculated. Afterwards, there was a comparison of every coefficient that was produced, in order to extract the highest value. Based on the highest spearman coefficient, the appropriate range was extracted and used further on.

The monotonic function returned by spearman's correlation is approximated by fitting a straight line on the correlated data. The form of the linear equation is described below

$$median = a \cdot th_{manual} + b$$

A relationship connecting median and threshold is now at hand. We also know both constants, a and b. Since what we are looking for is a way of calculating an automatic threshold for a new case, whilst a, b, and median are known, we proceed to solve the previous equation for th. We then have:

$$th_{auto} = \frac{median - b}{a}$$

By applying this equation on every unknown case of our set, we successfully receive an automatic threshold.

The following flowchart is indicative of the improved, optimized algorithm:

```
                    ┌─────────────┐
                    │    start     │
                    └─────────────┘
                           │
                           ▼
              ┌──────────────────────────┐
              │   load frames from 0     │
              │     sec and 144 sec       │
              └──────────────────────────┘
                           │
                           ▼
```

calculate
$$normalized(i) = \frac{blue(i) - green(i)}{255 - green(i)}$$
for every pixel i, on both frames

calculate median on
red channel

find automatic threshold
$$th = \frac{median - b}{a}$$

cut off image(i)<th

Overlay pseudocolor map on final
image0 and image144

```
                    ┌─────────────┐
                    │     end      │
                    └─────────────┘
```
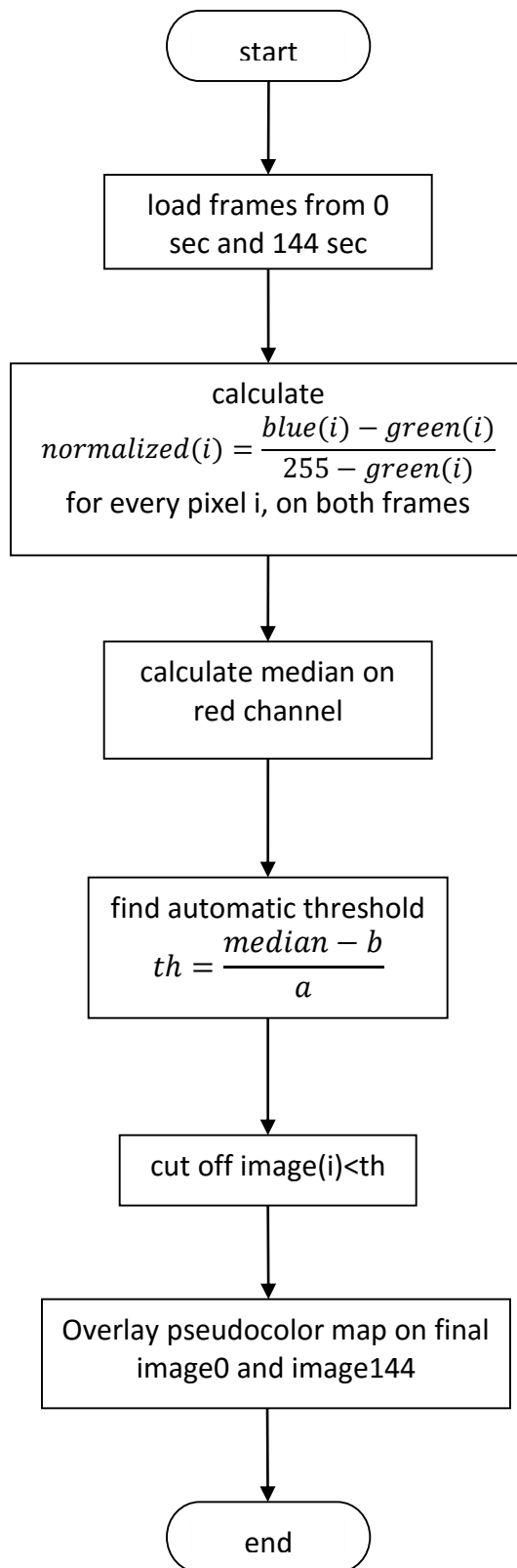
Figure 5.3-2 Flow chart of Physics based model Algorithm with automated thresholding
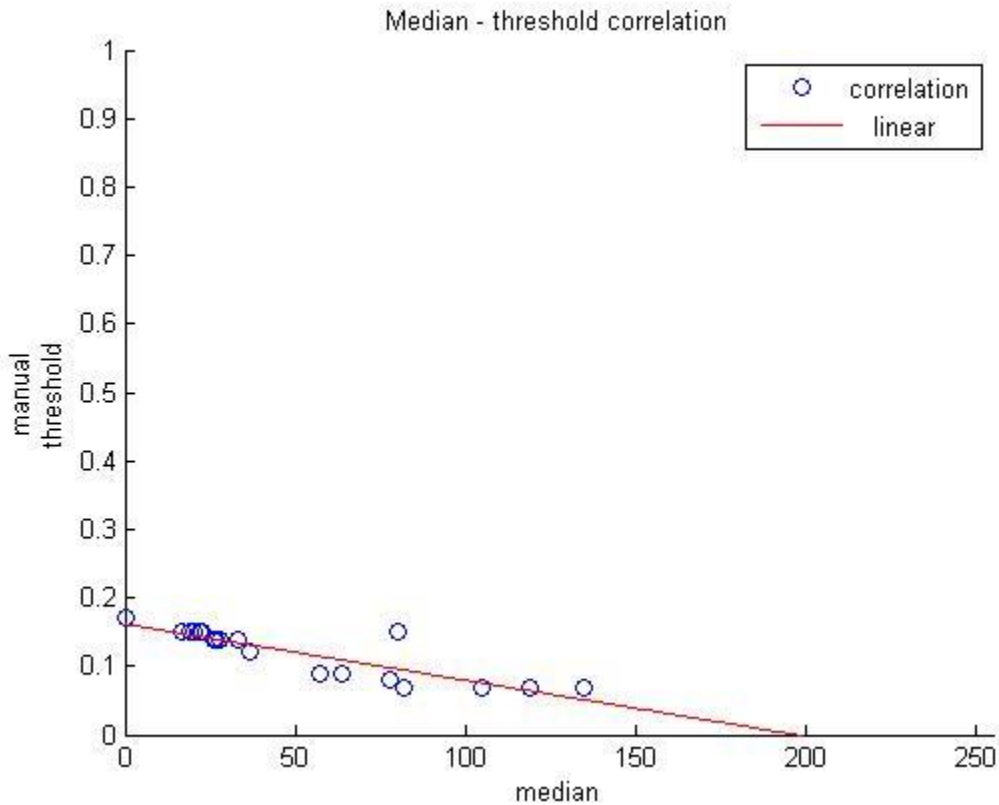
Figure 5.3-3 Correlation of median over manual thresholding and Approximation line

The scatter plot shown in Figure 5.3-3 shows the monotonic tendency between median and manual thresholds. Every blue point relates the median and the threshold of a given case. As we can see there is a tendency for decline; the greater the median the lower the threshold. It is clear that a strong, monotonic functions exists between the two sets. The red line is fitted on our data, in order to extract the linear coefficients.

5.4 Acetowhitening detection optimization

Although the algorithm so far, produces acceptable results, there is a highlighted need for distinguishing areas exhibiting leukoplakia and areas exhibiting acetowhitening phenomenon. Both leukoplakia and acetowhitening lesions appear white to the eye, posing a dilemma on correctly identifying pre-cancerous lesions.

Leukoplakia appears in cases where the squamous epithelium has plaques of keratin on its surface; the keratin prevents light from penetrating the upper cellular layers reducing backscattering light.

A ratio to further exploit the backscattering mechanism is introduced, in order to differentiate the areas of interest. The following ratio is used as a mask, on the RGB frame:

$$\text{mask(i)} = \frac{\text{blue(i)} - \text{green(i)}}{\text{blue(i)} + \text{green(i)}}$$

Where blue and green are the channels of the frame and i is a given pixel.
By breaking down the ratio and examining the limits of blue and green, we identify three distinct cases:
Assuming blue=0   ⇒ratio result equals -1
Assuming green=0   ⇒ratio result equals 1
Assuming blue=green   ⇒ratio result equals 0
We can see that the ratio will always result into values between [-1, 1].

By carefully examining the results of this ratio on the training set, it became clear that we can classify areas of the tissue according to the range of values. It seems that acetowhitening lesions always belong in the area [0, 0.3]. Based on this observation, we apply this mask as a first step of our algorithm, in order to exclude areas we are not interested in.

Considering the fact that the latter limits where calculated on the training set alone, in order to avoid bias, we had to loosen the range; our new relaxed limits are [-0.15, 0.45].
The mask previously described, is applied twice on our algorithm; it is the first and last step of our algorithm.

Initially, we apply the mask on the RGB frames, cutting of values outside the range [-0.15, 0.45]. A new RGB image is received, with our areas of interest, whereas the rest areas appear as black. We then proceed with the algorithm described previously. After the calculation of the automatic threshold and its application on the image, we perform once again the mask, with the strict limits of [0, 0.3], excluding any unnecessary information that might still exist.

The final, optimized algorithm is described in the following flowchart:

```
                          ┌─────────┐
                          │  start  │
                          └────┬────┘
                               │
                               ▼
                    ┌──────────────────────┐
                    │ Load frames from 0   │
                    │ sec and 144 sec      │
                    └──────────┬───────────┘
                               │
                               ▼
              ┌──────────────────────────────────┐
              │ calculate                         │
              │                                   │
              │            blue(i) − green(i)     │
              │  mask(i) = ─────────────────────  │
              │            blue(i) + green(i)     │
              │                                   │
              │  for every pixel i, on both frames│
              └──────────────┬───────────────────┘
```

calculate
$$mask(i) = \frac{blue(i) - green(i)}{blue(i) + green(i)}$$
for every pixel i, on both frames

cut off mask(i)<=-0.15 & mask(i)>=0.45

calculate
$$normalized(i) = \frac{blue(i) - green(i)}{255 - green(i)}$$
for every pixel i, on both frames

calculate median on red channel of image144

find automatic threshold
$$th = \frac{median - b}{a}$$

cut off image(i)<th

calculate
$$mask(i) = \frac{blue(i) - green(i)}{blue(i) + green(i)}$$
for every pixel i, on both frames

cut off mask(i)<=0 & mask(i)>=0.3

end

Figure 5.4-1 Flow chart of Physics based model Algorithm with automated thresholding and cut off masking

In confirmed low grade cases, even after the use of an automatic threshold, there is still unnecessary information kept. Therefore, by introducing a mask, whose purpose is to cut off any information unrelated to AW, we expect to see a significant improvement in low grade cases.

If we do not apply this mask, we can still identify high grade lesions but we seem to fail when it comes to low grade cases. Since all the previous steps provide good results for high grade lesions, we do not expect different results after the application of the mask.

We present the results before and after the application of the mask, on a low grade case.
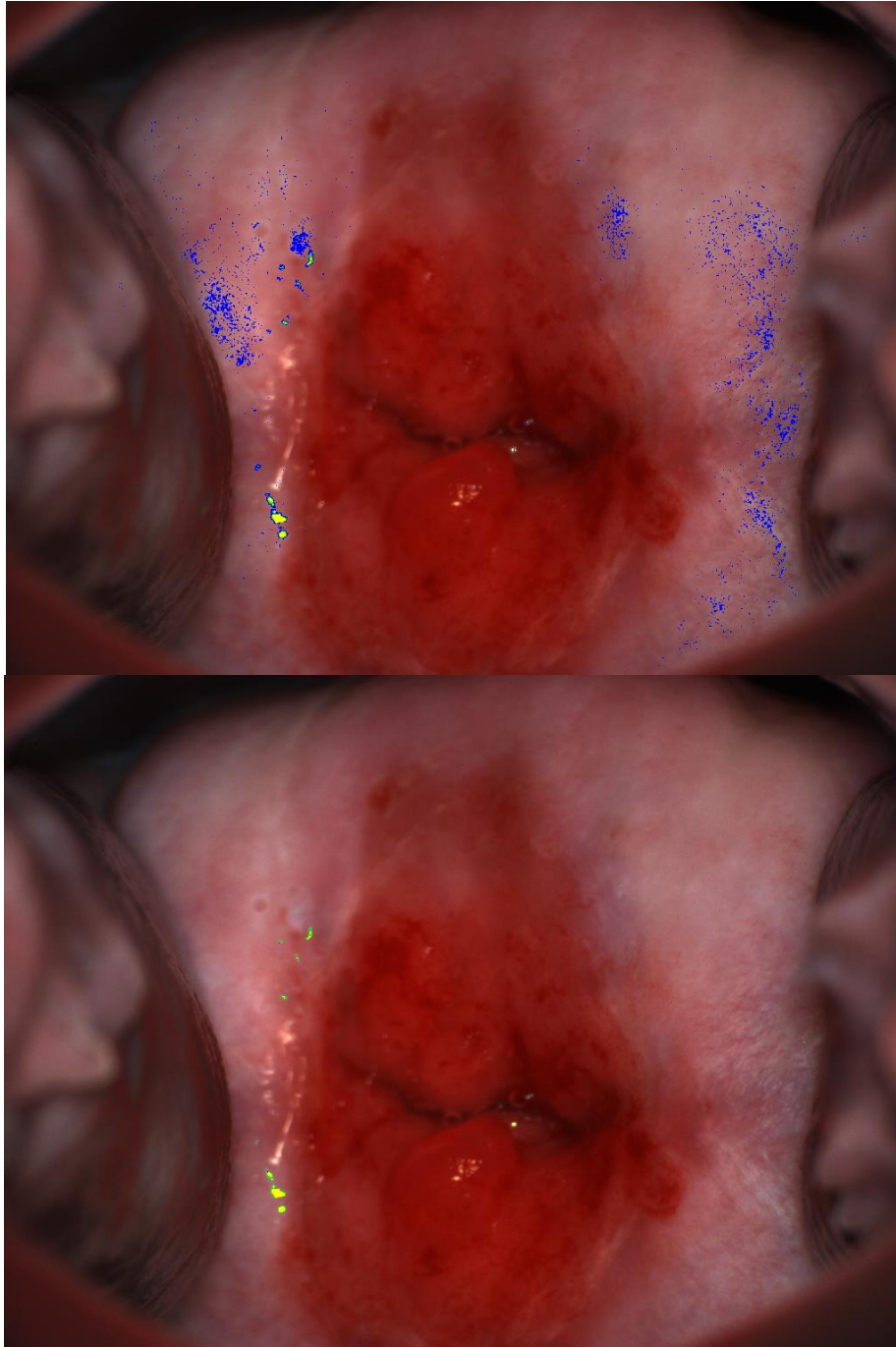
Figure 5.4-2 3 Captured frames with overlaid pseudocromatic map from confirmed low grade case, at frame at 0 seconds before application of acetic acid (above) without mask (below) with mask
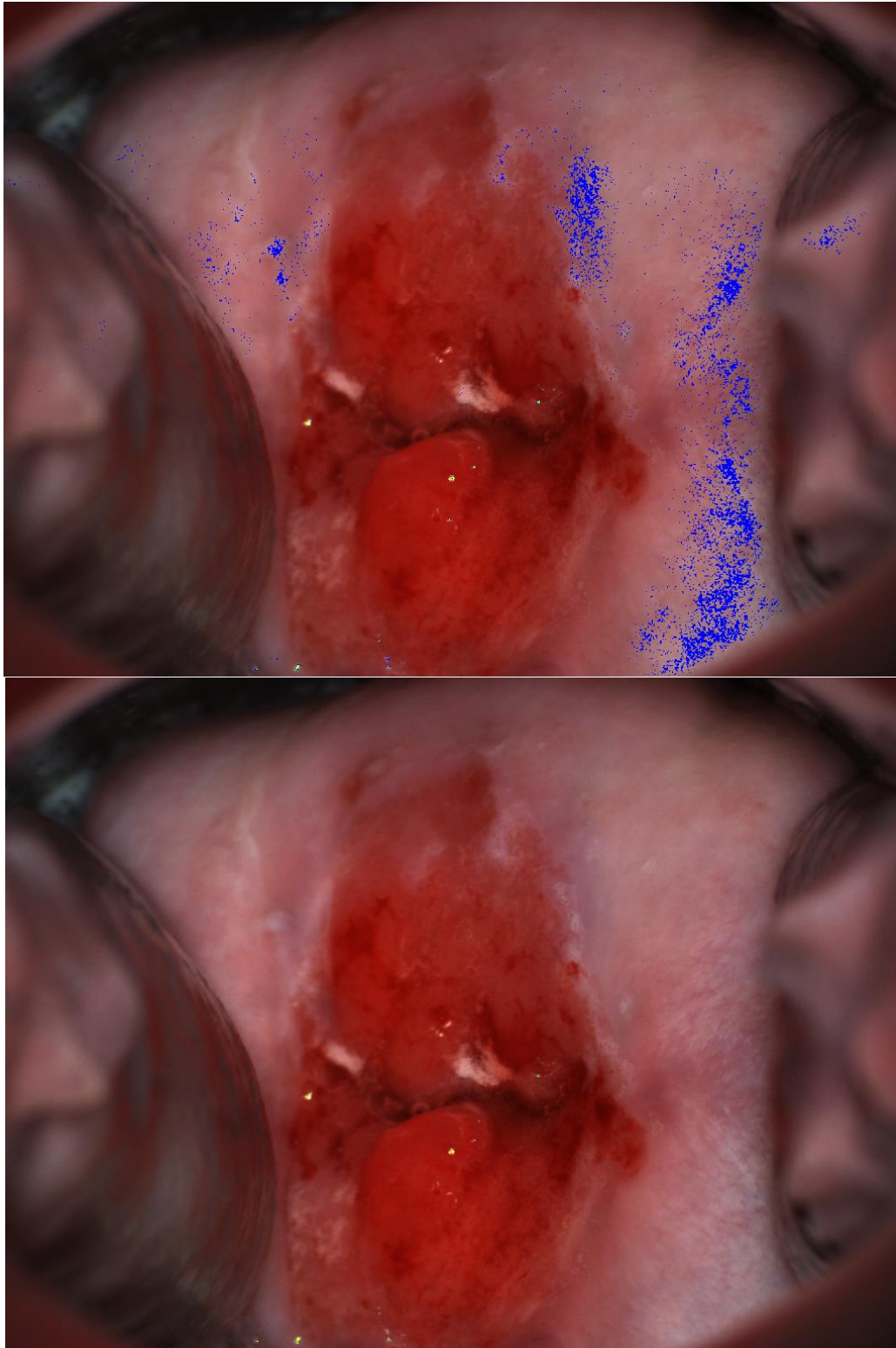
Figure 5.4-3 Captured frames with overlaid pseudocromatic map from confirmed low grade case, at frame at 144 seconds before application of acetic acid (above) without mask (below) with mask

As we can see from the previous figures, there is a significant improvement after the application of the mask. Dispersed pixels as well as irrelevant information are eliminated.

More importantly, the mask successfully distinguishes areas of leukoplakia and acetowhitening. This case is confirmed low grade. Visually there is a great area identified as white; this is a case with leukoplakia. When no mask is applied, the algorithm misinterprets the white areas as acetowhitening. When we apply the mask, the results correctly show this case as low grade.

6 Statistical analysis and Results

6.1 Statistical Analysis

Diagnostic tests are never perfect. False positive and false negative results occur. A new diagnostic test needs to be compared with the "gold standard", which in our case is the histology. In order to evaluate the algorithm's performance, it is imperative to apply a statistical analysis on the results. The accuracy of the algorithm is examined by measuring its capability to identify and grade the stages of the lesion.

The information obtained by comparing a new diagnostic test with the gold standard are summarized in a confusion matrix:

In cell "True Positive", we enter those who have the disease (as determined by the gold standard) and are correctly identified as such by the proposed algorithm of this thesis.

In cell "False Positive", we enter those who have been identified as patient by the proposed algorithm but do not have the disease according to the gold standard. In this case, the proposed algorithm has wrongly diagnosed the disease.

In cell "False Negative", we enter those who have been identified as diseased by the gold standard, yet the proposed algorithm has returned negative results. Therefore, a patient has been wrongly labeled as 'normal.

In cell "True Negatives", we enter those who have no disease as determined by the 'gold standard' and are also negative with the proposed algorithm.

We can now define some statistics to quantify how good a test is at picking out patients with the disease of interest. The two most commonly reported indicators are sensitivity and specificity [29-32].

Sensitivity is the proportion of truly diseased persons in the screened population who are identified as diseased by the screening test. This measure indicates the probability that the test will correctly diagnose a diseased person. The formula used to calculate sensitivity is:

$$\text{sensitivity} = \frac{\text{number of true positives}}{\text{number of truepositives} + \text{number of false negatives}}$$

Specificity is the proportion of the truly healthy people in the screening population who are identified as healthy by the screening test. It indicates the probability that the test will correctly identify a healthy person. The formula used to calculate specificity is:

$$\text{specificity} = \frac{\text{number of true negatives}}{\text{number of true negatives} + \text{number of false positives}}$$

To summarize, the higher the sensitivity, the greater is the capability of the test to identify patients with malignant lesions. On the other hand, the higher the specificity, the lower the misguidance of the test in normal cases.
Ideally, a test should have high sensitivity and high specificity. Sometimes there are tradeoffs in terms of sensitivity and specificity. For example, a test can have very high sensitivity, but this sometimes will result in low specificity.

6.2 Results

Using the validation set described in section 5.1, we performed a statistical analysis in order to evaluate the results of the algorithm. Every case was evaluated based on the pseudocolor map returned by the algorithm.

As a reference, we used the biopsy marks used during the clinical trial mentioned in section 2.4. By carefully examining every case, we graded the resuts as high grade or low grade; next, comparing our findings with the histologic results, we categorised our desicions as true positive, true negative, false positive or false negative.

Results were evaluated based on four different cases:

a) Using automatic threshold and pseudocolor map on biopsy points
b) Using automatic threshold and pseudocolor map on whole image
c) Using a default threshold of 0.07 and pseudocolor map on biopsy points
d) Using a default threshold of 0.07 and pseudocolor map on whole image

TP	FP
8	12
FN	TN
2	46
Sensitivity=0.8	Specificity=0.79

TP	FP
9	26
FN	TN
1	32
Sensitivity=0.9	Specificity=0.57

TP	FP
10	23
FN	TN
0	35
Sensitivity=1	Specificity=0.6

TP	FP
10	49
FN	TN
0	9
Sensitivity=1	Specificity=0.16

By comparing all four cases, we can observe that best results are obtained when an automatic threshold is used. By identifying the light intensity of every case, we obtain results strictly associated with the case at hand. Since every tissue and every lighting condition is unique, we observe that this is the best approach.

When it comes to the pseudomap, we can see that by evaluating the whole image, specificity tends to decline. The reason behind this is that many of the cases had artifacts caused by the speculum or by the presence of foam and/or mucus, therefore the pseudomap was not only associated with areas of AW.

If we use a universal threshold for every case, sensitivity and specificity both decline dramatically, since we do not take into account the uniqness of lighting conditions and tissue.

For all the reasons described above, it was decided that the best approach was the application of an automatic threshold.

From the four statistical evaluations of our algorithm, we can observe that the predefined global threshold achieves a 100% sensitivity, but with a severe trade off in specificity. This justifies the implementation and use of a methodology for automatic threshold. The results of the remaining two statistical evaluations reduce this trade off remarkably, retaining high performance.

Finally, we compare our results, 80% sensitivity and 79% specificity, with both DySIS™ and colposcopy. For the given set, DySIS™ achieved a sensitivity of 86% and specificity 94% whereas conventional colposcopy achieved a sensitivity of 62% and specificity of 89%.

Statistical results were also claculated without the use of the mask, in order to see if there is any improvement on the performance of the algorithm.

TP	FP		TP	FP
8	12		9	26
FN	TN		FN	TN
2	46		1	32
Sensitivity=0.8	Specificity=0.79		Sensitivity=0.9	Specificity=0.55

Although there is no significant difference in the statistical results, the use of this mask leads to a visually better map.

In overall, the algorithm has a very good behavior when it comes to identyfing high grade lesion. There is still potential for improvment; removal of glares and areas of foam, application of Spearman correlation on a larger training set are some of them.

In the pages that follow, we present the final maps for several indicatives cases, both high and low grade, as well as the results given by DySIS™ during the second clinical trial.

1. *Case 109   Confirmed CIN3*
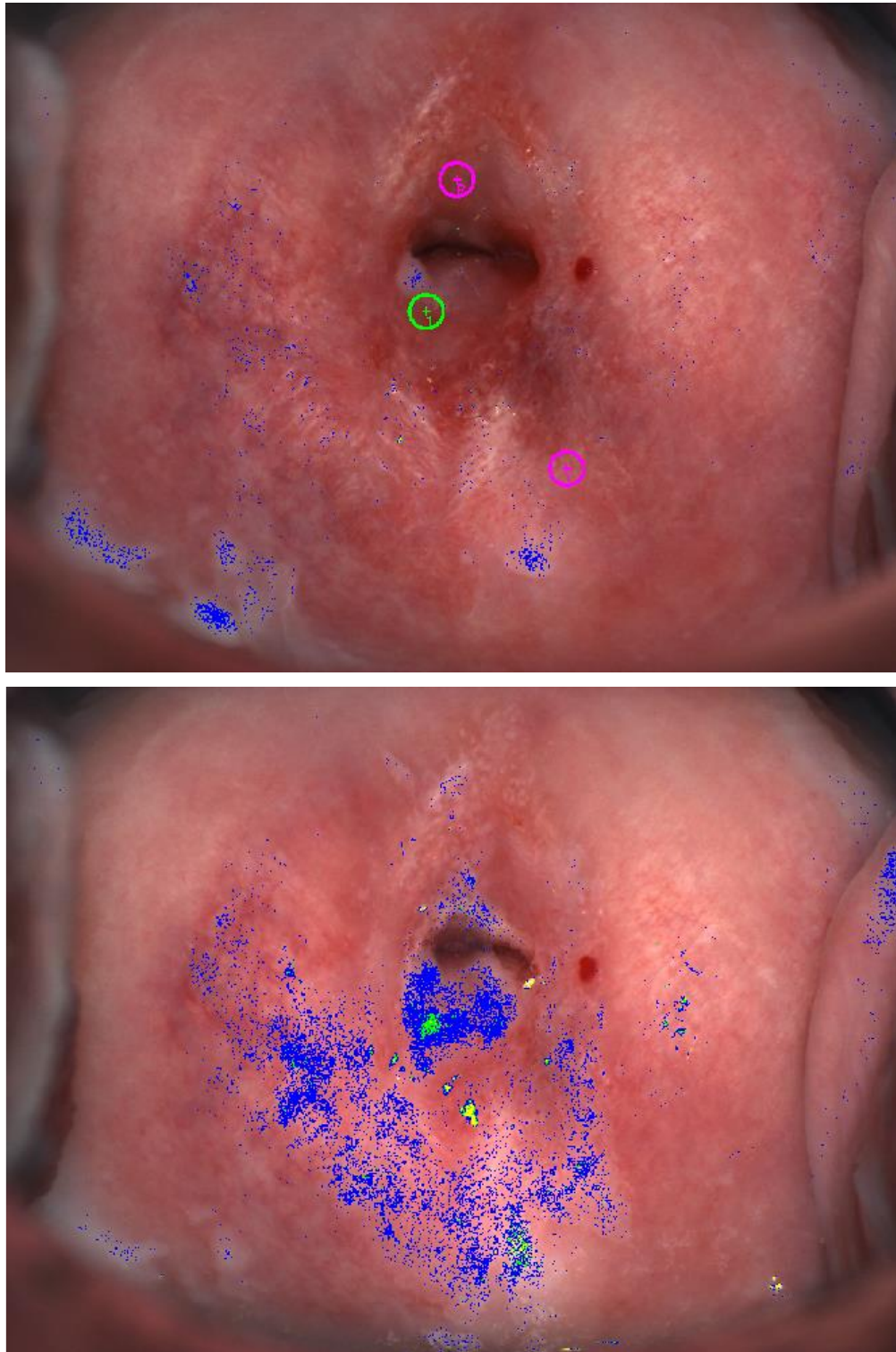
Figure 6.2-1 Captured frames, with overlaid pseudocolor map depicting intensified AW phenomenon, from confirmed high grade case 109 (above) frame at 0 seconds before application of acetic acid (below) frame at 144 seconds after the application of acetic acid
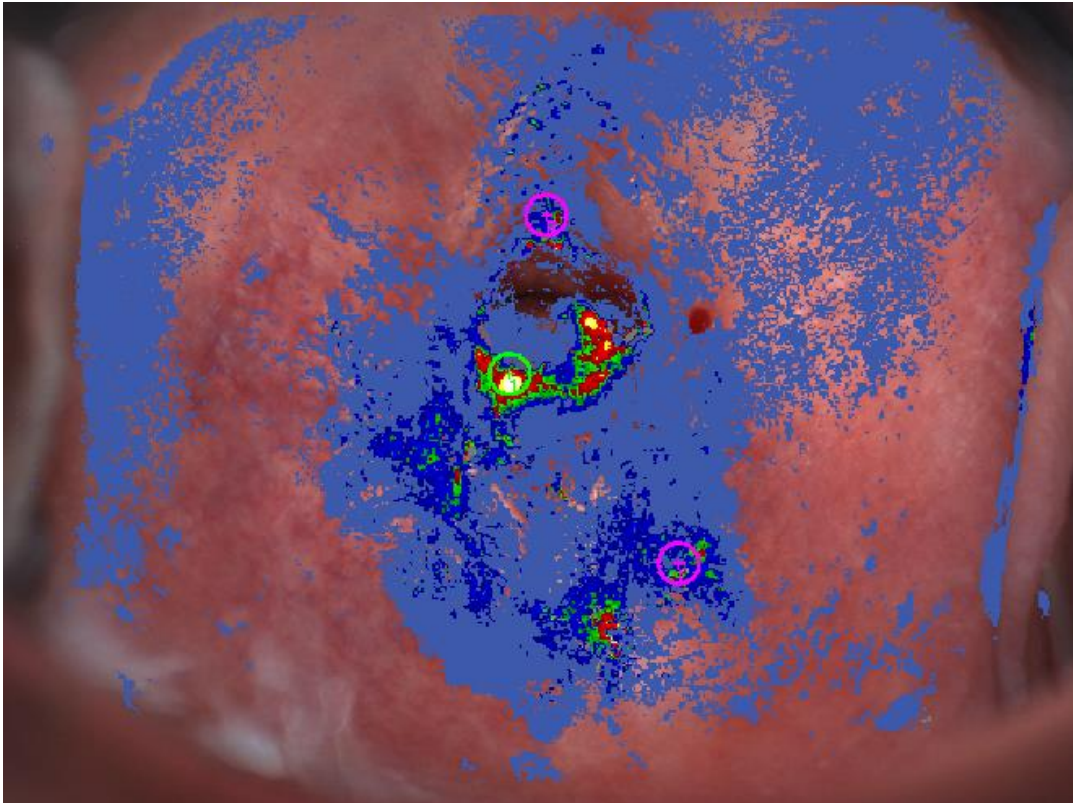
Figure 6.2-2 DySIS pseudocolor map for case 190

This case was confirmed by biopsy as HG. Figure 6.2-3 shows the results of our algorithm.

As we can see at figure 6.2-4, DySIS produces a colormap indicating a high grade lesion in areas that appear red and white. At the same time, our algorithm also produces a map, corresponding to the same areas as Dysis.

This case also has areas with leukoplakia; those areas are succesfully disregarted from our algorithm, thus no map exists at those areas.

Both methods have correctly identified the case as true positive.

2. Case 14　　　Confirmed CIN3
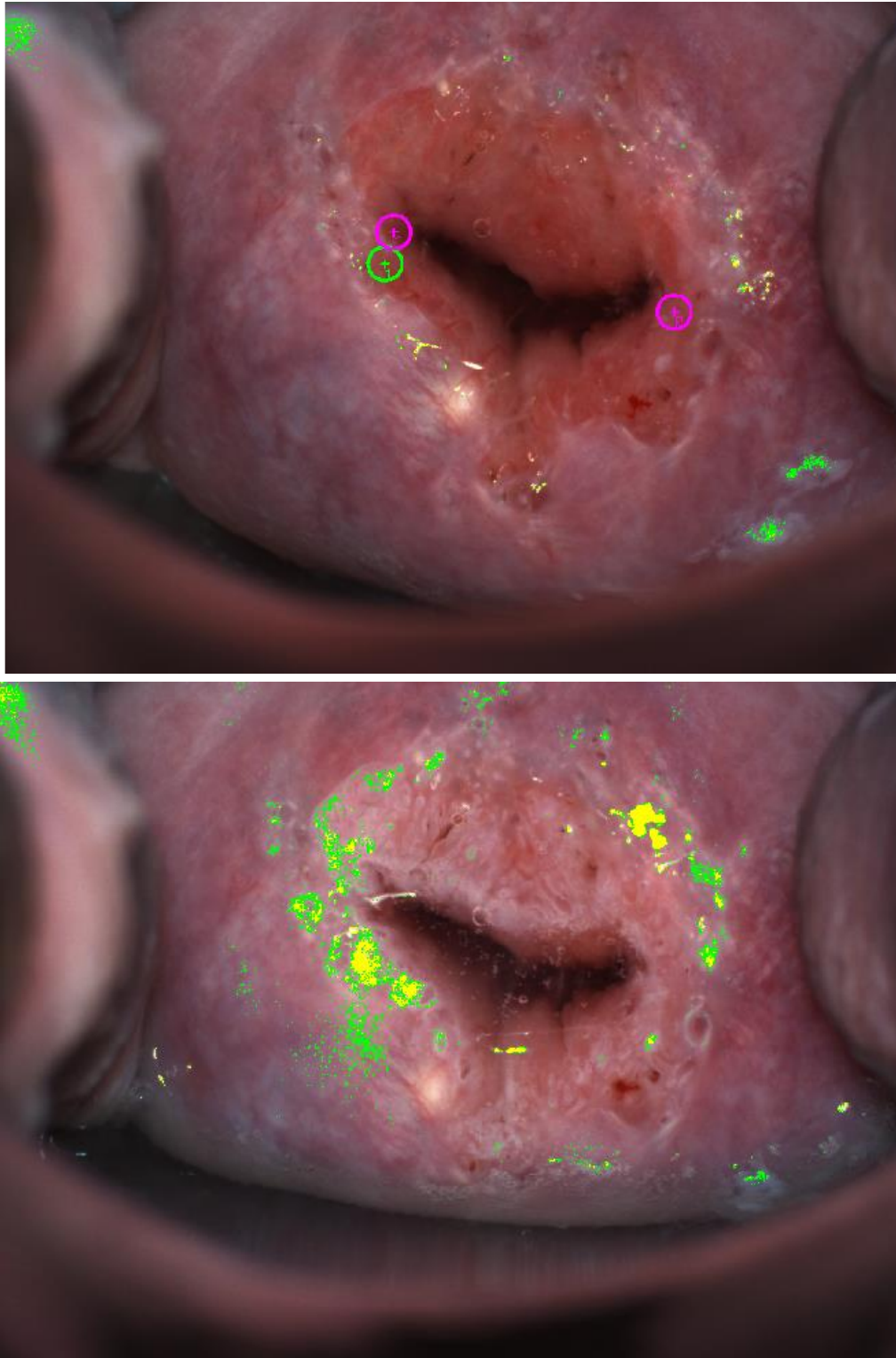
Figure 6.2-5 Captured frames, with overlaid pseudocolor map depicting intensified AW phenomenon, from confirmed high grade case 14 (above) frame at 0 seconds before application of acetic acid (below) frame at 144 seconds after the application of acetic acid
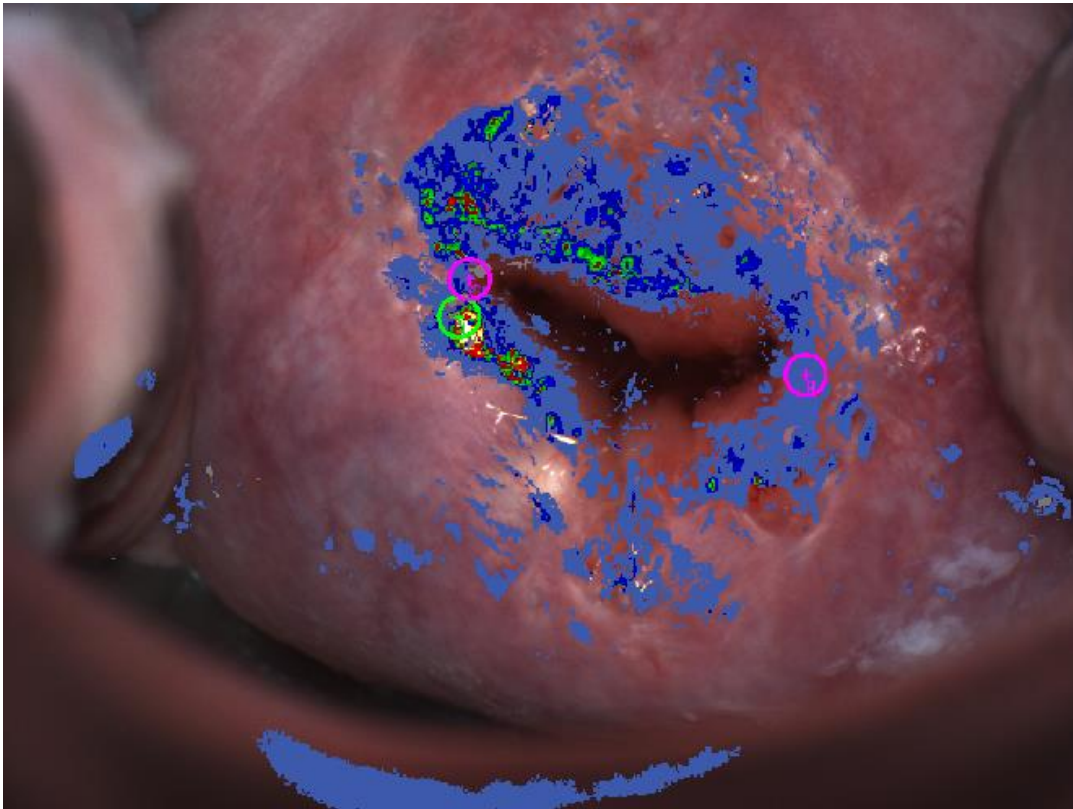
Figure 6.2-6 DySIS pseudocolor map for case 14

Case 14 was also confirmed by biopsy as HG. Figure 6.2-3 shows the results of our algorithm.

Comparing both maps, we can see that our algorithm correctly identifies the same areas as DySIS.

Both methods have correctly identified the case as true positive.

3. *Case 79   Confirmed CIN3*
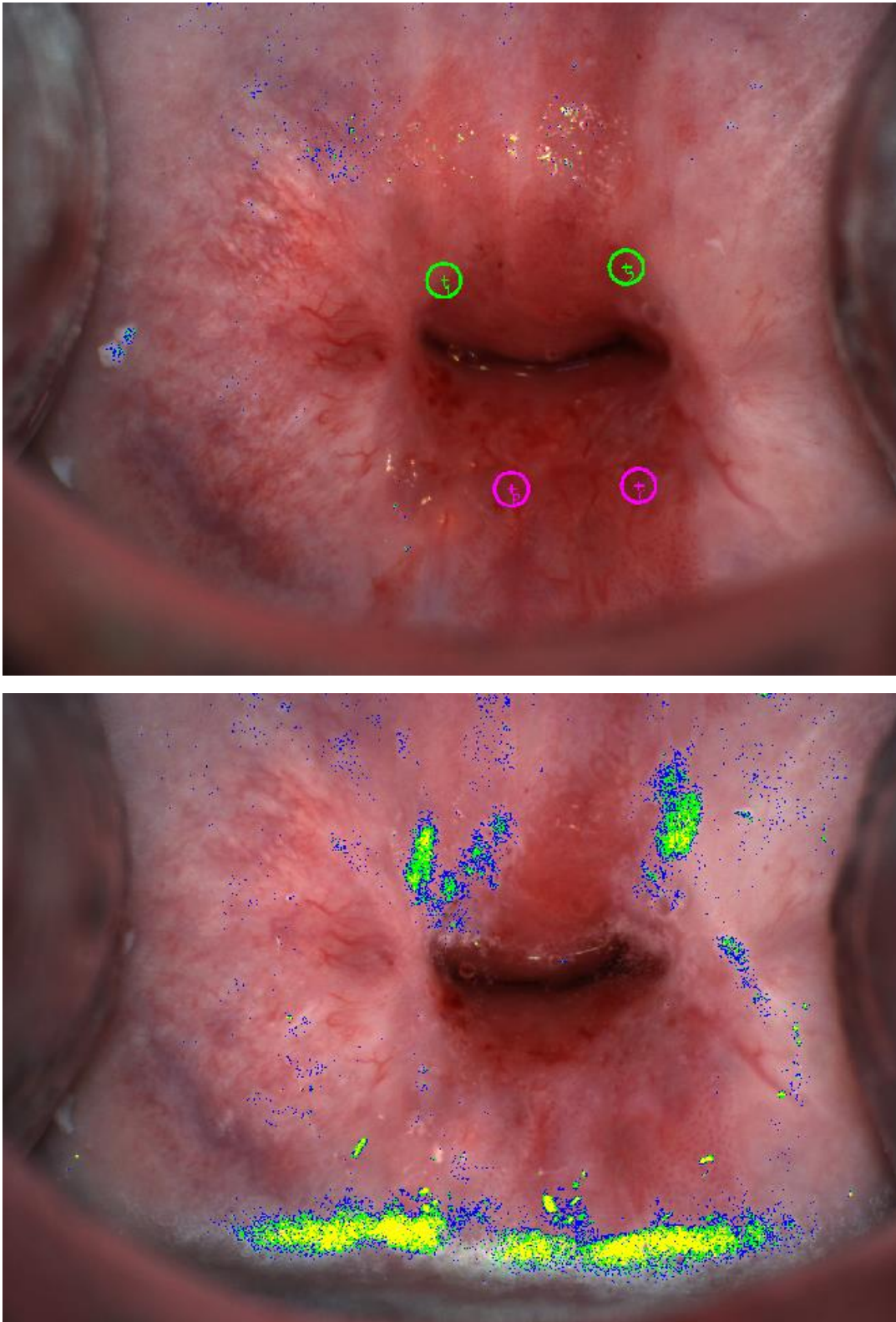
Figure 6.2-7 Captured frames, with overlaid pseudocolor map depicting intensified AW phenomenon, from confirmed high grade case 79 (above) frame at 0 seconds before application of acetic acid (below) frame at 144 seconds after the application of acetic acid
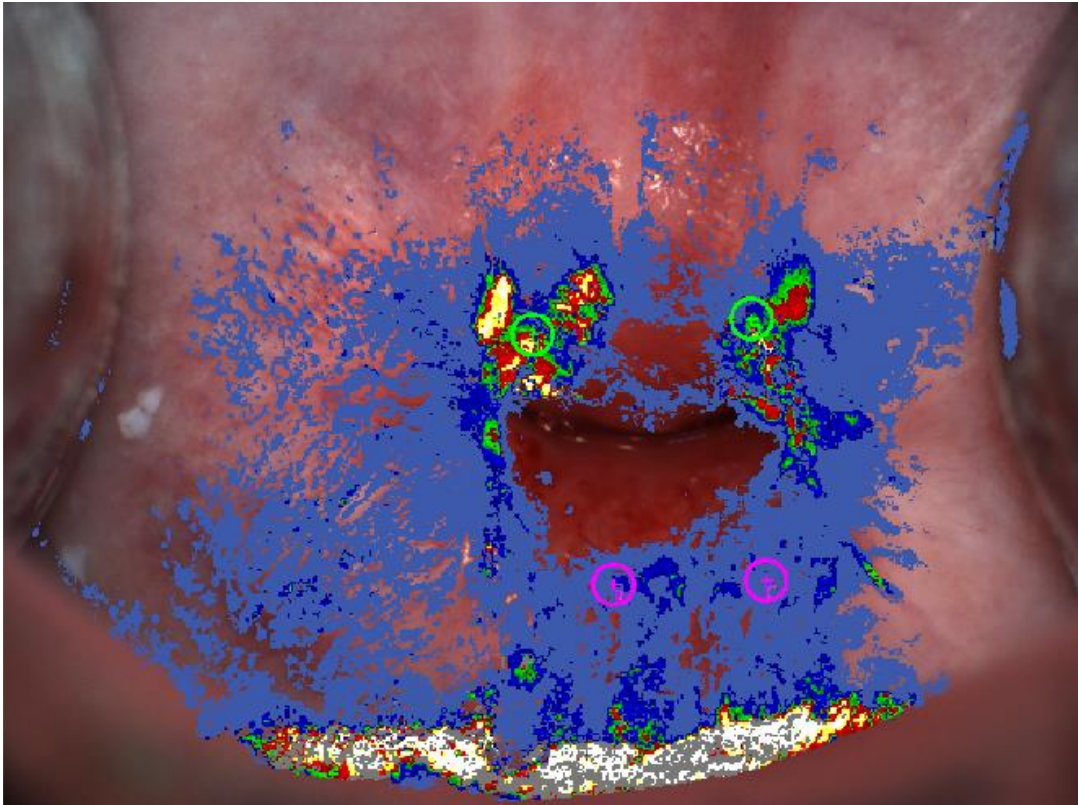
Figure 6.2-8 DySIS pseudocolor map for case 79

Case 79 is also confirmed by biopsy as HG. Figures .. and… show the results of our algorithm.

Our method has succesfully identified the same high grade areas as DySIS.

It is also important to mention that in this case there is a relatively big area covered with foam. Curently, no technique has been used, in this thesis, to disregart areas of foam. During the statistical analysis, map produced on areas covered with foam was not taken into account.

Both methods have correctly identified the case as true positive.

4. *Case 135   Confirmed CIN1*

Figure 6.2-9 Captured frames, with overlaid pseudocolor map depicting intensified AW phenomenon, from confirmed low grade case 135 (above) frame at 0 seconds before application of acetic acid (below) frame at 144 seconds after the application of acetic acid
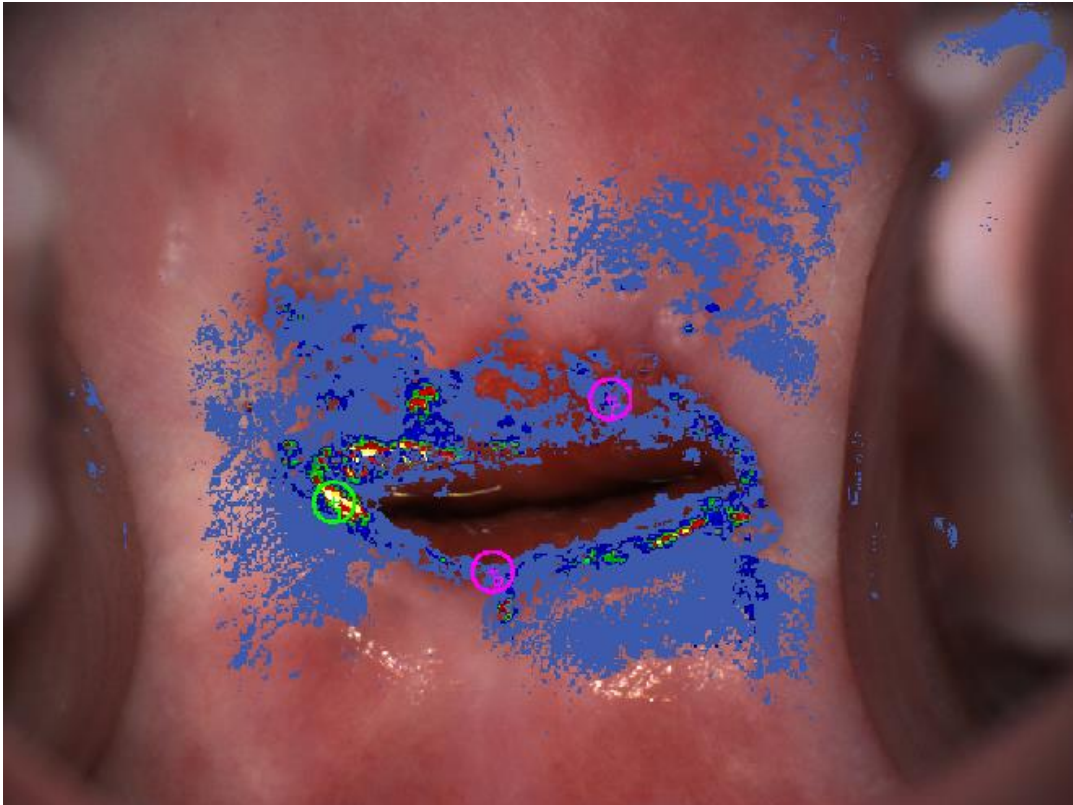
Figure 6.2-10 DySIS pseudocolor map for case 135

This is an especially important case, since it can show the success of our method. As we can see, DySIS has produced a map which indicates the presence of a high grade lesion. Our algorithm produces no map.

If we carefully examine the image144 of this case, we observe that the area that DySIS identifies as high grade, is actually covered with mucus. We conclude that DySIS has been mislead by artifacts, incorrectly identifying this case as high grade.

On the other hand, the algorithm we proposed does not exhibit this kind of behavior due to the biophysical background. Since the entire prosess is based upon tissue-light interaction and the mechanism of backscattering, cases like the present one are not misinterpreted.

To sum up, DySIS has concluded high grade, thus false positive, whereas our algorithm has concluded low grade, thus true negative.

5. *Case 45   Confirmed CIN1*
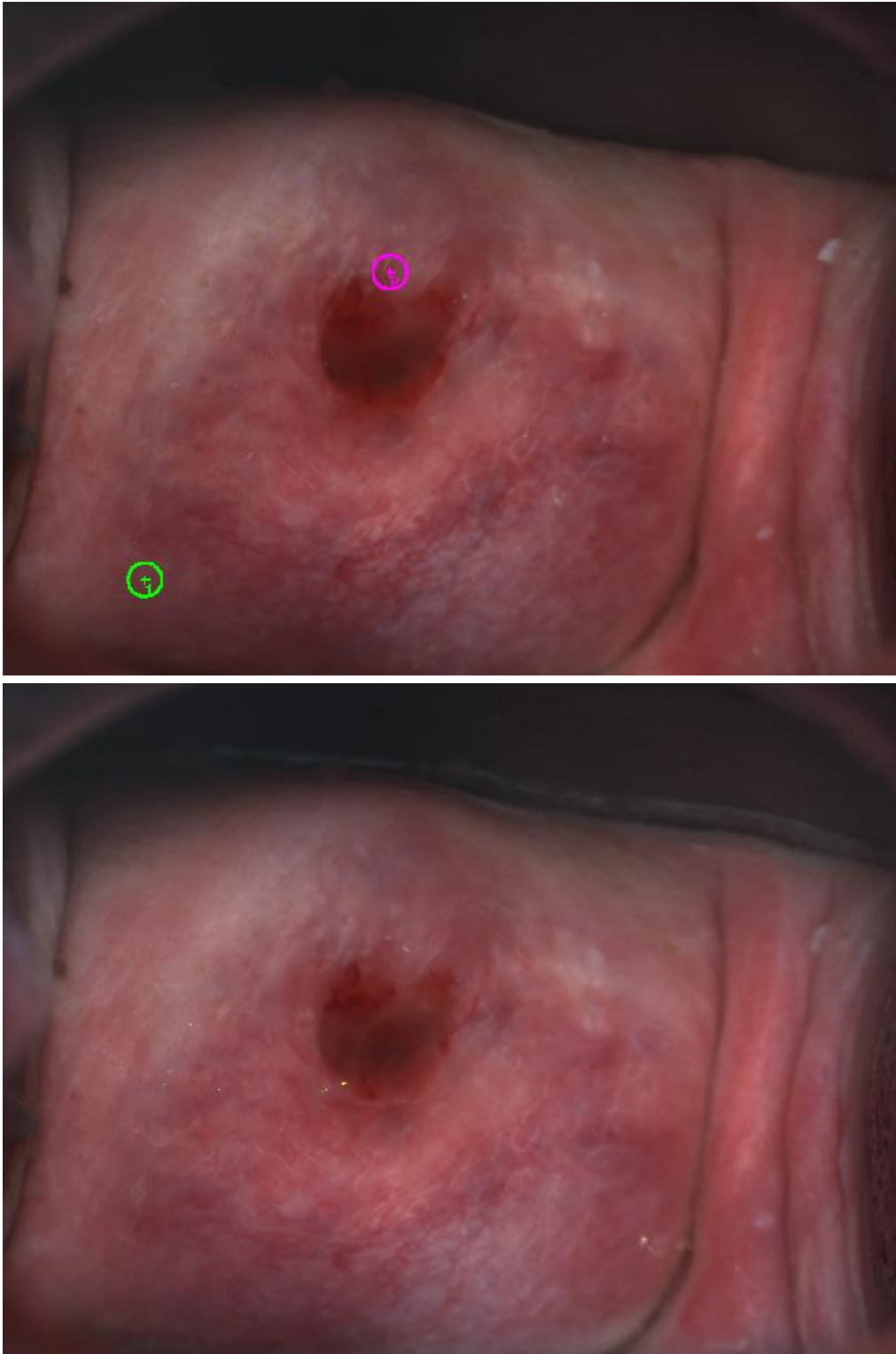
Figure 6.2-11 Captured frames, with overlaid pseudocolor map depicting intensified AW phenomenon, from confirmed low grade case 45 (above) frame at 0 seconds before application of acetic acid (below) frame at 144 seconds after the application of acetic acid
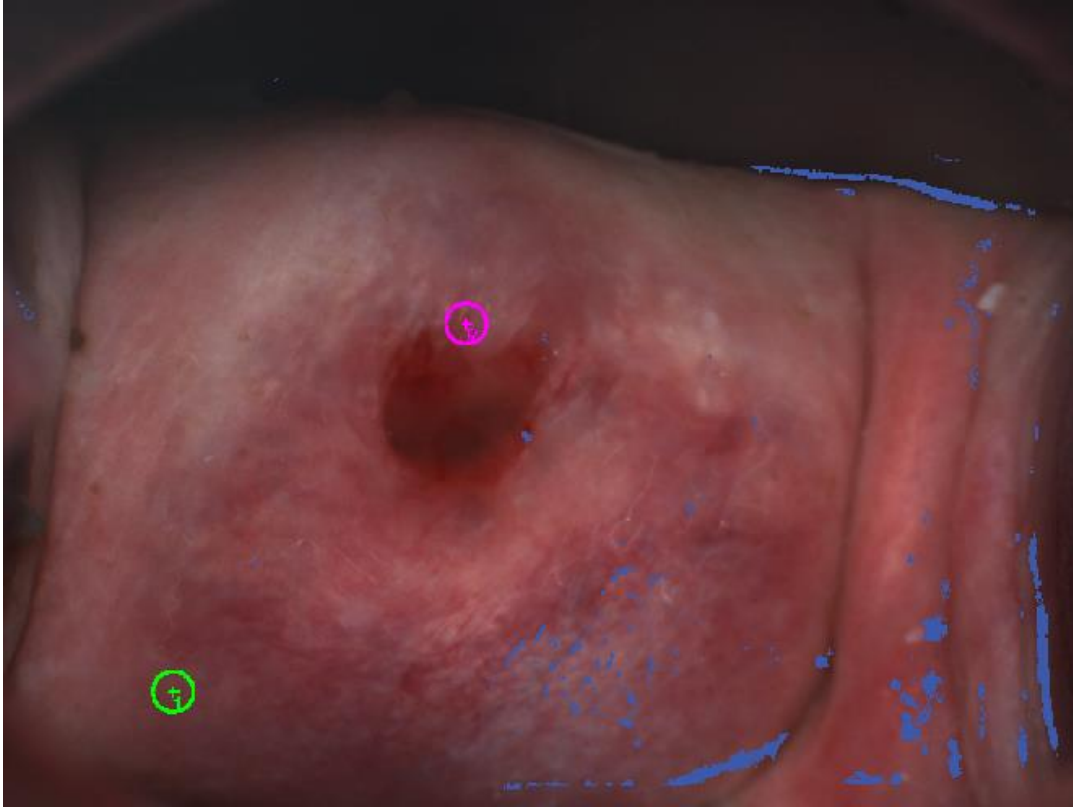
Figure 6.2-12 DySIS pseudocolor map for case 45

This is a relatively easy case, since both maps show no signs of high grade lesion. Both methods conclude that this case is low grade, as confirmed by the biopsy.

6. *Case 113   Confirmed CIN1*
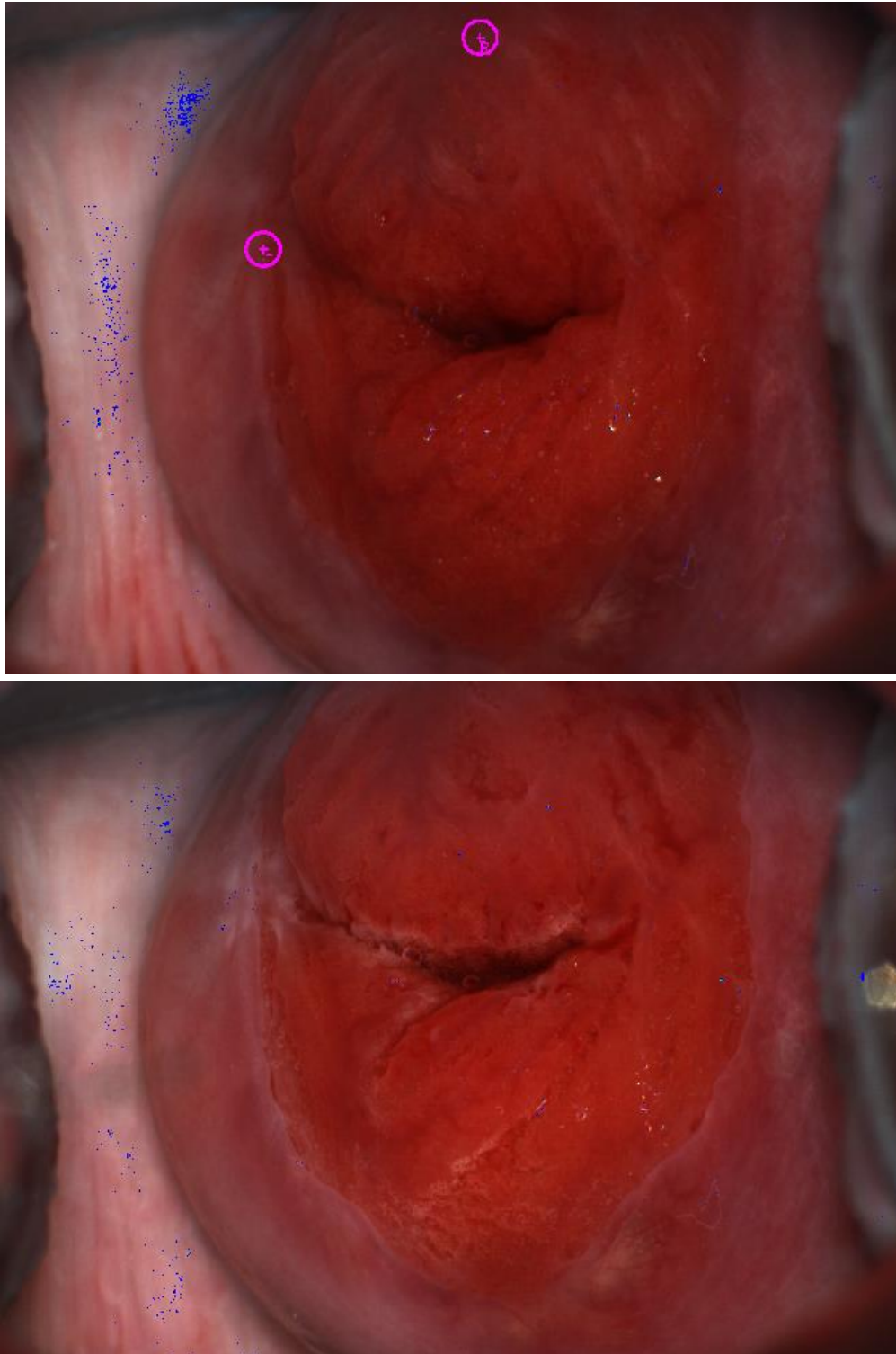
Figure 6.2-13 Captured frames, with overlaid pseudocolor map depicting intensified AW phenomenon, from confirmed low grade case 113   (above) frame at 0 seconds before application of acetic acid (below) frame at 144 seconds after the application of acetic acid
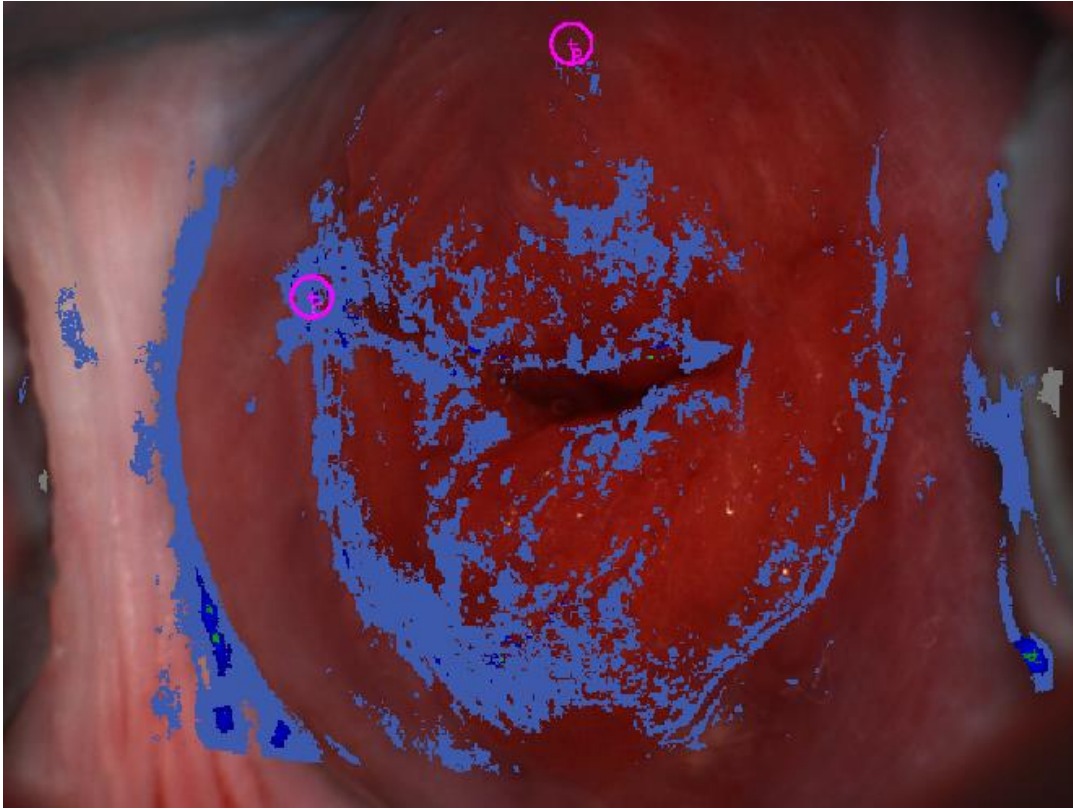
Figure 6.2-14 DySIS pseudocolor map for case 113

Similarily to the previous case, both methods correctly identify this case as low grade. The big difference is that DySIS produces a map, even though low grade, whereas our method shows no signs of lesions.

7 Epilogue

7.1 Conclusions

We have successfully implemented and presented a method, whose ability in detecting pre-cancerous lesion is of extreme importance.
After the assessment of our results and the comparison with the existing screening methods, we can see that we have achieved high, statistically significant, results with superior sensitivity to conventional colposcopy. We have objectively quantified and graded lesions without using redundant information.

One of the main reasons behind the implementation of the present algorithm, was the need for accurate and time-indepented diagnosis, omitting unnecessary procedures. Since one of the greatest disatvantages of the current diagnostic chains is the number of unnecessary performed biopsies, the proposed algorithm will be a great guiding tool for colposcopists.

The method we have presented, meets all the criteria and has every potential of evolving into a great diagnostic tool.

7.2 Future Work

Despite the great results of this method, there are still many aspects involving Dynamic Spectral Imaging, which can be examined. We have yet to discover the potential of observing the phenomenon in the ultraviolet or infrared portion of the spectrum, where it could be proven that it is possible to extract more information from the acetowhitening phenomenon.
Moreover there is high potential and promise in using acetic acid in combination with a new biomarker that stains tissue green.

Lastly, a greater training and validation set is required to further examine the potential of the algorithm. Therefore, the deployment of a device with the proposed algorithm and new clinical trials for the assessment of the instrumentation, are extremely imperative.

8 REFERENCES

[1] GLOBOCAN "Estimated Incidence, Mortality and Prevalence Worldwide in 2012"
http://globocan.iarc.fr/old/FactSheets/cancers/cervix-new.asp

[2] National Cancer Institute http://www.cancer.gov/types/cervical

[3] World Health Organization "Human papillomavirus (HPV) and cervical cancer"
http://www.who.int/mediacentre/factsheets/fs380/en/

[4] International Agency for Research on Cancer
Colposcopy and Treatment of Cervical Intraepithelial Neoplasia: A Beginner's Manual /
Chapter 2: An Introduction to Cervical Intraepithelial Neoplasia (CIN)

[5] American Cancer Society "New Screening Guidelines for Cervical Cancer"
http://www.cancer.org/cancer/news/new-screening-guidelines-for-cervical-cancer

[6] John Hopkins Medicine "Pap Test"
http://www.hopkinsmedicine.org/healthlibrary/test_procedures/gynecology/pap_test_
procedure_92,P07783/

[7] Canadian Cancer Society

[8] http://patient.info/doctor/colposcopy

[9] http://www1.cgmh.org.tw/intr/intr5/c6700/obgyn/f/web/Colposcopy/index.htm

[10] John Hopkins Medicine "Cervical Biopsy"
http://www.hopkinsmedicine.org/healthlibrary/test_procedures/gynecology/cervical_bi
opsy_92,p07767/

[11] American Cancer Society "The Papanicolaou test"
http://www.cancer.org/cancer/cervicalcancer/moreinformation/cervicalcancerpreventi
onandearlydetection/cervical-cancer-prevention-and-early-detection-pap-test

[12] Colposcopy and Cervical Punch Biopsy
http://www.healthcommunities.com/gynecological-tests/colposcopy-cervical-punch-
biopsy.shtml

[13] Patient information: Colposcopy
http://www.uptodate.com/contents/colposcopy-beyond-the-basics?source=see_link

[14] [Guide to Cervical Cancer
http://www.cancer.net/cancer-types/cervical-cancer/diagnosish

[15] Cervical Cancer In-Depth Report
http://www.nytimes.com/health/guides/disease/cervical-cancer/print.html

[16] http://mortakis.hpvinfocenter.gr/index.php/test-papanikolaou

[17] C.Balas, "A Novel Optical Imaging Method for the Early Detection, Quantitative Grading
and Mapping of Cancerous and Precancerous Lesions of Cervix", IEEE Trans. On
Biomedical Engineering, vol. 48, no. 1, Jan 2001

[18] Soutter et al, "Dynamic Spectral Imaging: Improving Colposcopy", Clin Cancer Res, vol.
15, no. 5, Mar 2009

[19] C.Balas, G.Papoutsoglou, A.Potirakis, "In Vivo Molecular Imaging of Cervical Neoplasia
Using Acetic Acid as Biomarker", vol. 14,no.1, Jan 2008

[20] Louwers J, Zaal A, Kocken M, ter Harmsel W, Graziosi G, Spruijt J, Berkhof J, Balas C,
Papagiannakis E, Snijders P, Meijer C, van Kemenade F, Verheijen R. Dynamic spectral

imaging colposcopy: higher sensitivity for detection of premalignant cervical lesions. BJOG 2010; DOI: 10.1111/j.1471-0528.2010.02806.x, Dec 2010

[21] Eurocytology "Anatomy, histology and function of the uterine cervix" http://www.eurocytology.eu/en/course/930

[22] An introduction to the anatomy of the uterine cervix http://screening.iarc.fr/doc/colpochapter01.pdf

[23] Anatomy of the cervix, squamocolumnar junction, metaplastic change and transformation zone http://www.gfmer.ch/ccdc/pdf/module1.pdf

[24] Teach me anatomy "The cervix" http://teachmeanatomy.info/pelvis/female-reproductive-tract/cervix/

[25] Cervical Histology and Infectious Diseases http://molpath.ucsd.edu/08-09HHMI%20Students/Summary_impact_09/HHMI_Renewal_Info/Kristyn%20Feldman%20Histology.pdf

[26] Book: "Berek & Novak's Gynecology", ,J.S. Berek, Fourteenth Edition, Lippincott Williams & Wilkins, 2007

[27] Book: "Introduction to the Human Body. The Essentials of Anatomy and Physiology" G.J. Tortora, B. Derrickson, 9th Edition

[28] Tao T. Wu and Jianan Y. Qu, "Assessment of the relative contribution of cellular components to the acetowhitening effect in cell cultures and suspensions using elastic light-scattering spectroscopy," Appl. Opt. **46**, 4834-4842 (2007)

[29] http://www.straighthealthcare.com/sensitivity-specificity-figure.html

[30] Explanation of Sensitivity and Specificity and How to Use Them http://getthediagnosis.org/definitions.html

[31] Parikh, R., Mathai, A., Parikh, S., Chandra Sekhar, G., & Thomas, R. (2008). Understanding and using sensitivity, specificity and predictive values. *Indian Journal of Ophthalmology*, *56*(1), 45–50.

[32] Interventional Studies Diagnostic Tests, Disease Screening Studies https://onlinecourses.science.psu.edu/stat507/node/71